NPEPPS is a novel and druggable driver of platinum resistance

Robert T. Jones[1,14], Mathijs Scholtes[2,14], Andrew Goodspeed[1,3,14], Maryam Akbarzadeh[2,5], Saswat Mohapatra[4], Lily Elizabeth Feldman[1], Hedvig Vekony[1], Annie Jean[1], Charlene B. Tilton[1], Michael V. Orman[1], Shahla Romal[5], Cailin Deiter[1], Tsung Wai Kan[2,6], Nathaniel Xander[1], Stephanie Araki[1], Molishree Joshi[1,7], Mahmood Javaid[8], Ryan Layer[8,9], Teemu D. Laajala[1,10], Sarah Parker[11], Tokameh Mahmoudi[2,5,6*], Tahlita Zuiverloon[2,*], Dan Theodorescu[4,12,13,*], and James C. Costello[1,3,15,*]

[1]Department of Pharmacology, University of Colorado Anschutz Medical Campus, Aurora, CO, USA
[2]Department of Urology, Erasmus MC Cancer Institute, Erasmus University Medical Center Rotterdam, Rotterdam, The Netherlands
[3]University of Colorado Cancer Center, University of Colorado Anschutz Medical Campus, Aurora, CO, USA
[4]Cedars-Sinai Samuel Oschin Comprehensive Cancer Institute, Los Angeles, CA, USA
[5]Department of Biochemistry, Erasmus University Medical Center Rotterdam, Rotterdam, The Netherlands
[6]Department of Pathology, Erasmus University Medical Center Rotterdam, Rotterdam, The Netherlands
[7]Functional Genomics Facility, University of Colorado Anschutz Medical Campus, Aurora, CO, USA
[8]Computer Science Department, University of Colorado, Boulder
[9]BioFrontiers Institute, University of Colorado, Boulder
[10]Department of Mathematics and Statistics, University of Turku, Turku, Finland.
[11]Smidt Heart Institute & Advanced Clinical Biosystems Research Institute, Cedars Sinai Medical Center, Los Angeles, California 90048, United States
[12]Department of Urology, Cedars-Sinai Medical Center, Los Angeles, CA, USA
[13]Department of Pathology and Laboratory Medicine, Cedars-Sinai Medical Center, Los Angeles, CA, USA
[14]Equal first authors
[15]Lead Contact
*Corresponding Authors

Corresponding Authors

Tokameh Mahmoudi, PhD
Departments of Pathology, Urology and Biochemistry
Erasmus University Medical Center
Dr. Molewaterplein 40, 3015GD, Rotterdam
The Netherlands
+31 6 53152973
t.mahmoudi@erasmusmc.nl

Tahlita Zuiverloon, MD, PhD
Department of Urology
Erasmus MC Cancer Institute, Erasmus University Medical Center
Dr. Molewaterplein 40, 3015GD, Rotterdam
The Netherlands

+31 6 26 41 90 87
t.zuiverloon@erasmusmc.nl

Dan Theodorescu, MD, PhD
Departments of Surgery and Pathology
Cedars-Sinai Medical Center
8700 Beverly Blvd. OCC Mezz C2002
7/3/23 11:05:00 PMLos Angeles, CA 90048
+1 (310) 423-8431
dan.theodorescu@cshs.org

James C Costello, PhD
Department of Pharmacology
University of Colorado Anschutz Medical Campus
Mail Stop 8303
12801 E. 17th Ave., Rm L18-6114
Aurora, CO 80045
+1 (303) 724-8619
james.costello@cuanschutz.edu

RUNNING TITLE
NPEPPS regulates platinum drug response

KEY WORDS
Puromycin-sensitive aminopeptidase; multi-omics; Synthetic Lethality; Chemoresistance; Bladder Cancer

FINANCIAL SUPPORT
This work was generously supported by the Anschutz Foundation to J.C.C., CA180175 to D.T., CA268055 to D.T. and J.C.C., FICAN Cancer Researcher by the Finnish Cancer Institute to T.D.L., Erasmus MC mRACE grant 111296 to T.Z., Erasmus MC fellowship project 107088 to T.Z., and training grants GM007635 and GM008497 supported R.T.J. This work utilized the Functional Genomics Facility, Biostatistics and Bioinformatics Shared Resource, Genomics Shared Resource, and Flow Cytometry Shared Resource supported by CA046934.

CONFLICT OF INTEREST STATEMENT
A provisional patent 63/153,519 has been filed on the subject matter of this work. J.C.C. is co-founder of PrecisionProfile and OncoRX Insight. All other authors declare no competing interests.

ABSTRACT

There is an unmet need to improve efficacy of platinum-based cancer chemotherapy. Using multi-omic assessment of cisplatin-responsive and -resistant human bladder cancer cell lines and whole-genome CRISPR screens, we identified Puromycin-Sensitive Aminopeptidase, NPEPPS, as a novel driver of cisplatin resistance. NPEPPS depletion sensitizes resistant bladder cancer cells to cisplatin *in vitro* and *in vivo*. Conversely, overexpression of NPEPPS in sensitive cells increased cisplatin resistance. We show that NPEPPS affects treatment response by regulating intracellular cisplatin concentrations. Patient-derived organoids (PDOs) generated from bladder cancer samples before and after cisplatin-based treatment, and from patients who did not receive cisplatin, were evaluated for sensitivity to cisplatin and they were found to be concordant with clinical response. In PDOs, shRNA depletion or pharmacologic inhibition of NPEPPS led to increased cisplatin sensitivity, while NPEPPS overexpression had the opposite effect. Our data present NPEPPS as a novel and druggable driver of cisplatin resistance by regulating intracellular cisplatin concentrations, along with providing the preclinical data to support clinical trials combining NPEPPS inhibition with cisplatin.

INTRODUCTION

Platinum-based chemotherapy has been successful in testicular, ovarian, bladder, head and neck, and lung cancer and remains a standard of care for many patients despite the advent of immunotherapy (1,2). However, dose-dependent side effects and chemoresistance have reduced the suitability and effectiveness of these drugs. The discovery of more effective agents or the development of strategies that improve efficacy of platinum-based regimens are approaches that can address these issues. Here we describe results from the latter approach, using bladder cancer (BCa) as a clinically relevant, and translationally tractable tumor models.

Bladder cancer accounts for 430,000 new diagnoses and 170,000 deaths worldwide annually (3). Cisplatin-based combination chemotherapy remains the first-line, standard of care for metastatic BCa, providing a 5-10% cure rate. However, up to 30% of patients are ineligible for cisplatin-based treatment (4) and are commonly offered immune checkpoint therapies (ICT) (5). However, ICT requires a PD-L1 diagnostic test, for which only ~25% of patients meet eligibility (6). Cisplatin-based combination chemotherapy is also standard of care in the neoadjuvant (NAC) setting for the management of localized muscle-invasive BCa (MIBC) (7,8). However, NAC adoption has been slow due to cisplatin toxicity and eligibility, along with the relatively small survival benefit of 5-15% over immediate cystectomy (9). Importantly, in both the metastatic and NAC settings, patient selection and therapeutic efficacy remain critical unresolved challenges (10).

Large-scale efforts have performed whole genome loss-of-function screening across hundreds of cancer cell lines using CRISPR- and shRNA-based libraries to define pan-cancer and context-specific genetic dependencies (11–14). While these efforts defined genetic dependencies in cancer, a limitation is that cells were grown under basal growth conditions in the absence of any treatment. Those studies were also performed in cells that had not acquired resistance to any treatments. To better understand the functional drivers of therapeutic resistance in the context of platinum drug treatment, here we performed CRISPR screens in the presence and absence of the therapy of interest (15–18), and in cells that have acquired resistance to the treatment itself (**Figure 1A**). Complementing these results with multi-omic profiling of treatment-responsive and -resistant cells allowed us to prioritize gene candidates for the best potential future clinical utility. Using these data, which make available as a public resource (https://bioinformatics.cuanschutz.edu/BLCA_GC_Omics/), we identified Puromycin-Sensitive Aminopeptidase, NPEPPS, as a novel driver of cisplatin resistance and validated this finding *in vitro* and *in vivo*. We then show that NPEPPS has its effect by directly regulating the intracellular concentrations of cisplatin. To determine the translational relevance of this discovery, tumor-derived organoids generated from patients before and after cisplatin-based chemotherapy, were used to validate and strengthen our results from bladder cancer cells and xenografts. In cells, xenografts, and organoids, we show that pharmacological inhibition of NPEPPS by tosedostat, a clinically used small molecule that inhibits NPEPPS, phenocopies genetic depletion of NPEPPS. Taken together our data supports NPEPPS as a therapeutic target and provides a compelling rationale for combining NPEPPS inhibition with cisplatin to improve bladder cancer patient outcomes.

MATERIALS AND METHODS

Cell Culture

All human BCa cell lines as reported in the Key Resource Table were obtained from the Resistant Cancer Cell Line (RCCL) Collection and were grown in Iscove's Modified Dulbecco's Medium (IMDM) with 10% Fetal Bovine Serum (FBS). Cells were passaged every two to three days. Resistance to gemcitabine and cisplatin was confirmed at the reported resistance doses from the RCCL (**Table S1** and **Figure S1**). Lentivirus production utilized 293FT cells (ThermoFisher), which were maintained in DMEM (high glucose) supplemented with 0.1mM non-essential amino acids (NEAA), 6mM L-glutamine, 1mM sodium pyruvate, and 500μg/mL geneticin (G418) with 10% FBS added. Cells were routinely monitored for mycoplasma and confirmed negative at multiple times during this study using MycoAlert (Lonza). All cells were grown at 37°C with 5% CO_2 in a humidified incubator.

All molecular characterization efforts (RNA sequencing, whole exome sequencing, and mass spectrometric proteomics) were performed on cells from independent passages and in drug-free, complete media to identify stable molecular changes rather than treatment-induced transient responses. Cells were routinely passaged through drug-containing media at the resistant doses (**Table S1**) to confirm resistance was maintained and early passage cells were utilized whenever possible.

RNA sequencing

Sample preparation

All cell lines were grown for several passages in the absence of antibiotics, gemcitabine or cisplatin. Cell pellets were snap frozen from sub-confluent dishes from 3 separate passages (replicates) for each of the 20 cell lines sequenced (5 cell lines, each with 4 derivatives: parental, G-resistant, C-resistant, GC-resistant). RNA was extracted using the RNAeasy Plus Kit (Qiagen). Cells were lysed and passed through QIAShredder column (Qiagen) according to the manufacturer's protocol. gDNA elimination columns (Qiagen) were used to remove any residual gDNA from the purified RNA. RNA integrity was assessed on the High Sensitivity ScreenTape Assay on the Tape Station2200 (Agilent) and only samples with an RIN score of 8 or higher were used for sequencing. RNA library preparation was performed using the Universal Plus mRNA –Seq +UDI kit (Nugen) according to the manufacturer's specification. Each library was sequenced to a minimum of 40 million clusters or 80 million 150bp paired-end reads on a NovaSeq 6000 instrument (Illumina) at the University of Colorado Cancer Center Genomics Shared Resource.

Data processing

Illumina adapters and the first 12 base pairs of each read were trimmed using BBDuk and reads <50bp post trimming were discarded. Reads were aligned and quantified using STAR (19) against the Ensembl human transcriptome (GRCh38.p12 genome (release 96)). Ensembl genes were mapped to HGNC gene symbols using HGNC and Ensembl BioMart. Gene counts were generated using the sum of counts for transcripts of the same gene. Lowly expressed genes were removed if mean raw count <1 or mean CPM (counts per million) <1 for the entire dataset. Reads were normalized to CPM using the edgeR R package (20). Differential expression was calculated using the voom function in the limma R package (21). In addition to two-group comparisons, single drug comparisons for all cell lines were generated with cell line as a covariate (**Table S9**).

197 ***Alignment and transcript quantification***

198 STAR --runThreadN 12 --runMode genomeGenerate --sjdbGTFfile
199 Homo_sapiens.GRCh38.96.gtf --genomeFastaFiles
200 Homo_sapiens.GRCh38.dna_sm.primary_assembly.fa
201
202 STAR --readFilesIn Read1.fastq.gz Read2.fastq.gz --readFilesCommand zcat --runThreadN 6 --
203 alignEndsProtrude 13 ConcordantPair --outFilterScoreMinOverLread 0.66 --
204 outFilterMatchNminOverLread 0.66 --outSAMtype BAM SortedByCoordinate --quantMode
205 GeneCounts
206

207 **Pathway analysis**

208 Gene set enrichment analysis was performed using the full list of genes ranked by fold change
209 for the indicated comparison and the fgsea R package (22) using gene sets from the Molecular
210 Signatures Database (v7.0) (23). General plots were generated with the ggplot2 and ggpubr R
211 packages (24). Heatmaps were generated with the ComplexHeatmap R package following z-
212 score transformation (25).

213

214 **Proteomics**

215 ***Sample preparation***

216 All cell lines were grown for several passages in the absence of antibiotics, gemcitabine or
217 cisplatin, then seeded at 100,000 – 200,000 cells per well and grown for 48 hours in IMDM +
218 10% FBS. Approximately 48 hours after seeding cells the supernatant was aspirated and cells
219 were washed 3 times with cold phosphate-buffered saline (PBS). Cells were lysed in 100μl of
220 8M Urea, 50mM Tris-HCl, pH 8.0. Lysates were transferred to pre-chilled 1.5mL microcentrifuge
221 tubes and centrifuged at 15000 RCF for 10 minutes to pellet. The supernatant was then
222 transferred to a clean, pre-chilled tube and frozen. Lysate replicates were collected in triplicate
223 from different passages. Cell pellets were lysed in 8M Urea supplemented with 0.1% Rapigest
224 MS compatible detergent. DNA was sheared using probe sonication, and protein concentration
225 was estimated by BCA (Pierce, Thermo Scientific). A total of 30μg protein per sample was
226 aliquoted, and samples were diluted to <2M Urea concentration using 200mM ammonium
227 bicarbonate while also undergoing reduction with DTT (10mM) and then alkylation with IAA
228 (100mM). The pH of diluted protein lysates was verified as between 7-8, and samples were
229 digested with sequencing grade Trypsin/Lys-C enzyme (Promega) in the presence of 10%
230 Acetonitrile for 16 hours at 37°C. Samples were acidified adding formic acid to 1%, and speed
231 vac dehydration was used to evaporate acetonitrile. Peptides were desalted on C18 tips (Nest
232 group) and dried to completion. Prior to MS, peptides were resuspended in 0.1% Formic Acid
233 solution at 0.5μg/μL concentration with 1:40 synthetic iRT reference peptides (Biognosys).

234 ***Data acquisition***

235 Peptides were analyzed by liquid chromatography coupled with mass spectrometry in data
236 independent acquisition (DIA) mode essentially as described previously (26). Briefly, 4μL of
237 digested sample were injected directly unto a 200 cm micro pillar array column (uPAC,
238 Pharmafluidics) and separated over 120 minutes reversed phase gradient at 1200 nL/min and
239 60°C. The gradient of aqueous 0.1% formic acid (A) and 0.1% formic acid in acetonitrile (B) was
240 implemented as follows: 2% B from 0 to 5 min, ramp to 4% B at 5.2 minutes, linear ramp to 28%
241 B at 95 minutes, and ramp to 46% B at 120 minutes. After each analytical run, the column was
242 flushed at 1200 nL/min and 60°C by injection of 50% Methanol at 95% B for 25 minutes followed

243 by a 10 minutes ramp down to 2% B and a 5 minute equilibration to 2% B. The eluting peptides
244 were electro sprayed through a 30 μm bore stainless steel emitter (EvoSep) and analyzed on an
245 Orbitrap Lumos using data independent acquisition (DIA) spanning the 400-1000 m/z range.
246 Each DIA scan isolated a 4 m/z window with no overlap between windows, accumulated the ion
247 current for a maximum of 54 seconds to a maximum AGC of 5E5, activated the selected ions by
248 HCD set at 30% normalized collision energy, and analyzed the fragments in the 200-2000m/z
249 range using 30,000 resolution (m/z = 200). After analysis of the full m/z range (150 DIA scans) a
250 precursor scan was acquired over the 400-1000 m/z range at 60,000 resolution.

251 ***Peptide library generation***

252 To construct a comprehensive peptide ion library for the analysis of human BCa we combined
253 several datasets, both internally generated and external publicly available data resources were
254 utilized. First, we utilized a previously published (27) human bladder tumor proteomics
255 experiment by downloading raw files from the online data repository (ProteomeXchange,
256 PXD010260) and searching them through our internal pipeline for data dependent acquisition
257 MS analysis (28) against the UniProt human reviewed canonical sequence database,
258 downloaded July 2019, using internal peptides to perform retention time alignment (29). To this
259 library, we appended a sample specific library generated from DIA-Umpire extraction of pseudo-
260 spectra from one full set of replicates from the experimental bladder tumor cell lines. A final,
261 combined consensus spectrast library containing all peptide identifications made between the
262 internal and external dataset was compiled and decoy sequences were appended.

263 ***Data analysis***

264 Peptide identification was performed as previously described in (28,29). Briefly, we extracted
265 chromatograms and assigned peak groups using openSWATH (30) against the custom BCa
266 peptide assay library described above. False discovery rate for peptide identification was
267 assigned using PyProphet (31) and the TRIC (32) algorithm was used to perform feature-
268 alignment across multiple runs of different samples to maximize data completeness and reduce
269 peak identification errors. Target peptides with a false discovery rate (FDR) of identification <1%
270 in at least one dataset file, and up to 5% across all dataset files were included in the final
271 results. We used SWATH2stats to convert our data into the correct format for use with
272 downstream software MSstats (33). Each individual data file was intensity normalized by
273 dividing the raw fragment intensities by the total MS2 signal. MSstats (33) was used to convert
274 fragment-level data into protein-level intensity estimates via the 'quantData' function, utilizing
275 default parameters with the exception of data normalization, which was set to 'FALSE'. For
276 plotting purposes, protein intensities were VSN normalized, log-transformed, and replicate batch
277 effects were removed using the removeBatchEffect function in the limma R package. The limma
278 package was also used to calculate differential protein expression (21). Multiple hypothesis
279 correction was performed using the Benjamin Hochberg method.

280

281 **Whole exome sequencing**

282 ***Sample preparation***

283 All cell lines were grown for several passages in the absence of antibiotics, gemcitabine, or
284 cisplatin. Cell pellets were snap frozen from sub-confluent dishes for each of the 20 cell lines
285 sequenced (5 cell lines, each with 4 derivatives: parental, Gem-resistant, Cis-resistant, GemCis-
286 resistant). gDNA isolation was performed using the Puregene cell and tissue kit (Qiagen) with
287 the addition of RNase A Solution (Qiagen) according to manufacturer's instructions. gDNA was
288 quantified using a Qubit 4.0, then sheared using a Covaris S220 Sonicator to 200bp. Libraries
289 were constructed using the Sure Select All Exon v6 library kit (Agilent) following the XT library

preparation workflow. Completed libraries were run on the 4200 Tape Station (Agilent) using D1000 screen tape. Libraries were quantitated using the Qubit, diluted to 4nM prior to verification of cluster efficiency using qPCR, then sequenced on the NovaSeq 6000 instrument (Illumina) (150bp, paired-end) at the University of Colorado Cancer Center Genomics Shared Resource. Mean insert size across all cell lines was 177.8 bp and mean coverage was 193.7X with > 96.8% at >30X. Individual call line quality control metrics are reported in **Table S11**.

Data processing

The analysis pipeline was developed using Nextflow. For the raw fastq files, Fastqc was used to assess overall quality. For computational efficiency, raw sequence reads were partitioned using BBMap (partition.sh) into 40 partitions. They then were aligned to the GRCh38 reference genome (including decoy sequences from the GATK resource bundle) using the BWA-MEM short read aligner (34), and merged back into single BAM files using Samtools. The resulting BAM files were de-duplicated using Samblaster (35), and sorted using Samtools. These duplicate-marked bams were further passed through the GATK Base Quality Score Recalibration in order to detect systematic errors made by the sequencing machine when it estimates the accuracy of base calls. The dbSNP (version 146) (36), the 1000 Genome Project Phase 1 (37), and the Mills and 1000G gold standard sets (38) were used as databases of known polymorphic sites to exclude regions around known polymorphisms from analysis. After alignment, Samtools (39), Qualimap (40), and Picard tools (41) were run to acquire various metrics to ensure there were no major anomalies in the aligned data.

Alignment

```
bwa mem -K 100000000 -R "read_group" -t 64 -M ref_fasta read_1 read_2
```

Marking duplicates

```
samtools sort -n -O SAM sample_bam | samblaster -M --ignoreUnmated
```

Base Quality Score Recalibration

```
gatk BaseRecalibrator -I sample_bam -O sample.recal.table -R ref_fasta --known-sites
known_sites
```

Whole exome sequencing variant calling

We used Mutect2 from the GATK toolkit for SNVs and short indels (42). Mutect2 is designed to call somatic variants and makes no assumptions about the ploidy of samples. It was run in *tumor-only* mode to maximize the sensitivity albeit at the risk of high false positives. We used tumor-only mode to call variants for each cell line separately. Mutect2 workflow is a two steps process. In the first step, it operates in high sensitivity mode to generate intermediate callsets that are further subjected to filtering to generate the final variant calls. Annotation of variants was performed using Annovar (43) with the following databases: refGene, cytoBand, exac03, avsnp150, clinvar_20190305, gnomad211_exome, dbnsfp35c, cosmic90. Intergenic variants were removed along with variants that were identified at greater than 0.001% of the population according to ExAC or gnomAD, or had a depth < 20.

Mutect2 raw callset:

```
gatk Mutect2 -R ref_fasta -I bam_tumor -tumor Id_tumor --germline-resource germline_resource
-O raw_vcf
```

Mutect2 filtering:

```
gatk FilterMutectCalls -V raw_vcf --stats raw_vcf_stats -R ref_fasta -O filtered_mutect2_vcf
```

333 ***Copy number calling using GATK***

334 Base quality score recalibrated bams were used as the input. The covered regions for the
335 exome kit were converted into bins (defining the resolution of the analysis) for coverage
336 collection. Read-counts, that form the basis of copy number variant detection, were collected for
337 each bin. The read-counts then go through denoising, modelling segments, and calling the final
338 copy ratios.

339 ***Preprocess intervals***

340 gatk PreprocessIntervals --intervals intervals_bed_file --padding 0 --bin-length 0 -R ref_fasta --
341 interval-merging-rule OVERLAPPING_ONLY -O preprocessed_intervals_list

342 ***Collect read counts***

343 gatk CollectReadCounts -I sample_bam -L preprocessed_intervals} --interval-merging-rule
344 OVERLAPPING_ONLY -O sample.counts.hdf5

345 ***Denoise read counts***

346 gatk DenoiseReadCounts -I sample.counts.hdf5 --standardized-copy-ratios
347 sample_std_copy_ratio --denoised-copy-ratios sample_denoised_copy_ratio

348 ***Model Segments***

349 gatk ModelSegments --denoised-copy-ratios denoised_copy_ratio --output-prefix id_sample -O
350 output_dir

351 ***Call copy ratio segments***

352 gatk CallCopyRatioSegments -I sample.modelled_segments -O sampled.called.segments

353 ***Cell line authentication***

354 Variant calls from the Mutect2 pipeline were filtered for each cell line to identify high confidence
355 variants according to the filtering criteria above. These high confidence variants were then
356 compared to the variants reported for all cell lines in the DepMap (https://depmap.org/portal/) for
357 the Cancer Cell Line Encyclopedia (CCLE_mutations_hg38.csv, sample_info.csv) and COSMIC
358 (CosmicCLP_MutantExport.tsv) as measured by the jaccard distance, the intersection of
359 variants divided by the union of variants. Cells listed in CCLE or COSMIC were the rank ordered
360 for each BCa cell line in this study according to the jaccard distance. Results are reported in
361 **Table S12**.

362

363 **Cell Line Drug Treatments**

364 Gemcitabine (Sigma) and cisplatin (Sigma) stocks were resuspended in 0.9% PBS solution. All
365 stock solutions were stored protected from light and kept frozen until use. For cell culture dose
366 response, cells were seeded in 96-well tissue culture plates with 500-2000 cells per well
367 depending on the growth rate and duration of the experiment. Cells were seeded and allowed to
368 attach overnight followed by replacing the media with fresh, pre-warmed media just prior to
369 treatment. Drug dilutions were performed serially and using complete media (IMDM + 10% FBS)
370 and the associated drug treatments. Growth inhibition was measured using confluence
371 estimates over time on the IncuCyte ZOOM (Essen Bioscience) over varying amounts of time
372 depending on each experiment. Dose response curves were generated with Prism v9.3.1 using
373 a variable slope, four parameter nonlinear regression model. Comparison between treatment
374 groups was done between IC50 values using the sum-of-squares F test. Details for timing and
375 replicates for each experiment are included in their respective figure legends.

Antibodies and Western Blotting

Whole cell lysates were prepared from cultured cells using RIPA lysis and extraction buffer (ThermoScientific). Lysates from xenograft tissues were prepared using tissue protein extraction reagent (T-PER) and glass tissue homogenizer. All lysates were prepared on ice and with the addition of Halt protease and phosphatase inhibitor cocktail and EDTA (ThermoFisher). Protein concentration of lysates were quantified with BCA protein assay (Pierce™, ThermoFisher). All lysates were prepared with 4X Licor Loading buffer with 50mM DTT added boiled for 10 minutes prior to gel loading. All western blots were run using PROTEAN TGX precast 4-15% or 4-20% gradient gels (Bio-Rad) and transferred to either 0.2μm or 0.44μm nitrocellulose membranes. Transfer was done for 1.5-2hrs in cold TrisGlycine buffer (Bio-Rad) with 20% methanol prior to blocking for 1hr at room temperature in 5% BSA in TBS-T. Primary antibodies were diluted and incubated overnight at 4°C on a rocker. Membranes were washed 3 or 4 times in fresh TBS-T prior a 1-hour room temperature incubation in an appropriate secondary antibody. Membranes were washed 3-4 times in TBS-T, developed with enhanced SuperSignal West Pico Plus or SuperSignal West Fempto (ThermoFisher), and imaged using Li-Cor Odyssey® Fc instrument. Densitometry was performed using LiCor Image Studio™ software. Statistical comparisons using densitometry measurements were done using a one-way ANOVA with Tukey post hoc to control for the experiment-wise error rate.

Western Blot Primary Antibodies:

Target	Vendor	Catalog number	Dilution	Type
GAPDH	Cell Signaling	5174S	1:1000	Rabbit polyclonal
H2AX	Thermofisher	MA1-2022	1:1000	Mouse monoclonal
NPEPPS	Thermofisher	PA5-83788	1:1000	Rabbit polyclonal

Western Blot Secondary Antibodies:

Target	Vendor	Catalog number	Dilution	Type
Goat-anti-Rabbit(HRP)	Abcam	ab97057	1:20,000	Goat polyclonal
Rabbit-anti-Mouse(HRP)	Sigma	A9044-2ML	1:10,000	Rabbit polyclonal

shRNA-mediated knockdown experiments

Lentiviral production and transduction were carried out by the University of Colorado Cancer Center Functional Genomics Shared Resources. Plasmids from The RNAi Consortium (TRC) collection (TRC construct numbers TRCN0000073838, TRCN0000073839 and TRCN0000073840) were used for targeting NPEPPS were selected based on predicted knockdown efficiency; non-targeting controls used were SHC002 and SHC016. 2μg of target shRNA construct and 2μg of 3:1 ratio of psPAX2 (Addgene) and pMD2.G (Addgene) were transfected into HEK293FT cells using 2 μg of Polyethylenimine (Polysciences). Lentiviral particle containing media was filtered using 0.45μm cellulose acetate syringe filter and used for transduction. Puromycin selection was performed at doses used for CRISPR library screening or in some cases, cells were re-selected with higher doses of puromycin (10μg/mL), in order to ensure the complete elimination of non-transduced cells. Selected cells were frozen at early passage and early passage cells were used for all experiments.

Intracellular cisplatin measurements using CyTOF

413 Cell lines were cultured for several passages in IMDM + 10% FBS. Prior to the experiment, cells
414 were cultured in IMDM10 to be 50-80% confluence overnight and then treated the next day with
415 10μM cisplatin or PBS and then dissociated after 4 hours of treatment. For dissociation, cells
416 were washed twice with room temperature PBS and then incubated with PBS + 0.05% Trypsin-
417 EDTA for 10-15 minutes. Cells were neutralized with IMDM10 and then fully dissociated into
418 single-cell suspension by gentle pipetting. After dissociation, cells were counted by Trypan blue
419 staining and then placed in separate tubes at 3 x 10^5 cells. Individual samples were then fixed,
420 permeabilized, and labeled using unique barcodes using the Cell-ID 20-plex Pd Barcoding kit
421 (Fluidigm) according to the manufacturer's protocol. Barcoded samples were pooled across cell
422 line conditions and cisplatin concentration, incubated with Cell-ID Intercalator-Ir, mixed with
423 equilibration beads, and acquired on a Helios mass cytometer (Fluidigm). Post-acquisition data
424 were normalized to equilibration beads and debarcoded, using the bead-normalization and
425 single-cell-debarcoder packages from the Nolan Laboratory GitHub page
426 (https://github.com/nolanlab). Relative cisplatin intensity (defined by ^{195}Platinum isotopic mass
427 intensity) was analyzed among nucleated ^{191}Iridium+ ^{193}Iridium+ events defined by Boolean
428 gating within FlowJo 10.7.1.
429

430 **Whole Genome CRISPR Screening**

431 ***Plasmid library expansion and quality control***

432 Whole genome CRISPR Screening was performed using the Human CRISPR Knockout Pooled
433 Library (Brunello) - 1 vector system (Addgene and a gift from John Doench to the Functional
434 Genomics Facility at the University of Colorado Anschutz Medical Campus)(44). Two distinct
435 plasmid expansions were performed. And the library distribution was assessed using next
436 generation sequencing to determine the impact on overall library was modest following re-
437 expansion. Library width was calculated as previously described(45,46) by dividing the 10th
438 percentile of the library distribution by the 90th percentile using the log2 average expression of
439 all sgRNAs in the library and found to be 6.7 and 7.13 for batch 1 and 2 respectively. All quality
440 control metrics for each sample are reported in **Table S13**. Different screening parameters were
441 used based on the cell line screened these are summarized in **Table S4.**

442 ***Lentivirus Production and Titration***

443 For the two plasmid batches, two distinct protocols for lentivirus production were utilized. The
444 first batch was generated by using Polyethylenimine, linear (PEI; Polysciences) and was used
445 for the T24-GemCis and TCCSUP-GemCis screens. The second used lipofectamine 3000 and
446 was applied for the 253J-GemCis, KU1919-GemCis, and 5637-GemCis screens. For the first
447 batch, 293FT cells were seeded at a density of 36,800 cells/cm^2 into a 4-layer CELLdisc
448 (Greiner) using DMEM + 10% FBS along with antibiotic and antimycotic solution. Transfection
449 mix consisting 47.6μg pMD2G (Addgene), 95.2μg of psPAX2 (Addgene), and 190.5μg of
450 Brunello Whole genome knockout library (Addgene) was mixed with 448μl PEI (1 mg/mL) and
451 3mL OptiMEM, vortexed for 30 seconds and allowed to incubate at room temperature for 20
452 minutes. Fresh media containing transfection mix were added to the CELLdisc using up to
453 270mL of media. The next day media was changed for 280mL fresh media followed by a 48-
454 hour incubation. After this 48-hour incubation the viral supernatant was harvested and filtered
455 through a cellulose acetate filter system (ThermoScientific) and frozen at -80°C.

456 The first method had low functional virus titer, so we implemented a different virus production
457 method for subsequent screens. In the second batch of virus production, we utilized
458 lipofectamine 3000 instead of PEI, eliminated use of multilayer flasks and centrifuged to remove
459 debris as opposed to filtering. Briefly, 293FT cells were plated in T225 flasks to be 80%
460 confluent after 24hrs. 2hrs before transfection, media was changed and 40mL of fresh media

461 was used per T225 flask. The lipofectamine 3000 protocol was followed according to
462 manufacturer's instructions and scaled based on the volume of virus being prepared. For each
463 T225 flask 2mLOptiMEM was mixed with 40μg Brunello whole genome library plasmid, 30μg of
464 psPAX2 and 20μg of pMD2.G and 180μl of P3000. This mix was added to a tube containing
465 2mL OptiMEM and 128μl Lipofectamine 3000, which was scaled according to the number of
466 T225 flasks being prepared. Transfection mix was mixed thoroughly by pipetting up and down
467 slowly, and allowed to incubate at room temperature for 15 minutes. Transfection mix was then
468 added dropwise to the plates of 293FT cells with gentle swirling and incubated overnight
469 (~16hr). The following morning, the media was changed and 60mL of fresh media was added to
470 each T225 flask. This was allowed to incubate overnight and replaced the following morning.
471 This first lentiviral supernatant was stored at 4°C to be pooled with a subsequent 48 hour
472 collection. Upon collection, viral supernatants had 1M HEPES added at 1%. Following the
473 second virus collection, supernatants were pooled and centrifuged at 1250rpm for 5 minutes to
474 pellet debris. Lentivirus was stored in polypropylene tubes as polystyrene is known to bind
475 lentivirus, and all tubes were flash frozen in liquid nitrogen and stored at -80°C. Despite the
476 changes to the lentiviral production protocols, functional lentiviral titers were not improved using
477 these changes to the methodology, but feel it is worth noting these changes in protocol to
478 account for any possible variability associated with this change.

479 Lentivirus was titered functionally based on protocols adapted from the Broad Institute's Genetic
480 Perturbation Platform's public web portal (https://portals.broadinstitute.org/gpp/public/).

481

482 ***Screening Parameter Optimization***

483 All screening parameters for each cell line including cell polybrene and puromycin sensitivity,
484 screening coverage, technical and biological replicates performed, and gemcitabine and
485 cisplatin treatment concentrations are reported in **Table S4.**

486 ***DNA Isolation***

487 Cell pellets of 2e7 were snap frozen in liquid nitrogen in 1.5mL tubes and stored at -80 prior to
488 extraction. When possible, at least 8e7 cell were used for 4 separate genomic DNA isolation
489 which were pooled to account for any variation with pellet size. DNA isolation was performed
490 using the Puregene cell and tissue kit (Qiagen) with the addition of RNase A Solution (Qiagen)
491 according to the manufacturer's instructions. DNA concentration was measured in quadruplicate
492 using either a nanodrop spectrophotometer (Thermo), Qubit® dsDNA assay (Life
493 Technologies), and the average DNA content per cell was determined.

494 ***Library preparation***

495 The minimum number of cell equivalents of gDNA to maintain equal coverage was used for
496 library preparation. In all screens, the minimum coverage based on cell number was multiplied
497 by the average gDNA content per cell for each individual cell line to determine the minimum
498 number for 10μg PCR reactions needed to maintain coverage. A minimum coverage of 500-fold
499 per sgRNA in the library was targeted for each independent sample or replicate but this was
500 increased in some cases where screening was carried out with greater depth (see **Table S4** for
501 coverage and replicate information).

502 Library preparation was performed using primers sequences designed by the Broad Institute's
503 Genetic Perturbation Platform (https://portals.broadinstitute.org/gpp/public/) and utilized a pool
504 of eight P5 primers with to introduce a stagger in reads associated with each library and sample
505 specific P7 primer that contained a unique sample index sequence for each timepoint, replicate,

506 or treatment condition to be sequenced in the same pool (**Table S14**). All library preparation
507 primers were resuspended at 100μM.

508 Each library preparation PCR reaction contained the following components: 1μl Herculase II
509 Fusion Enzyme (Agilent), 2.5μl Deoxynucleotide (dNTP) Solution Mix (New England Biolabs),
510 0.5μl P5 primer pool, 0.5μl P7 index primer, 20μl 5X Reaction Buffer (Agilent), 10μg of gDNA
511 and nuclease-free water to bring the total reaction volume to 100μl. Samples underwent 23
512 cycles of thermal cycling followed by a quality assessment by electrophoresis on 2% agarose
513 gel to ensure consistent library amplification across multiple wells and samples for each plate.

514 Each unique library had 10μl pooled from all PCR reactions performed on that unique sample
515 and mixed thoroughly. 50-100μl of the pooled library preparation reactions was used to perform
516 magnetic bead-based purification and elimination of any residual free primer using a 0.8X ratio
517 SPRIselect beads (Beckman Coulter) according to the manufacturer's instructions. Libraries
518 were then assessed for appropriate amplicon size and complete elimination of free primer peaks
519 using the High Sensitivity ScreenTape Assay on the Tape Station2200 (Agilent) and quantified
520 using the qPCR-based quantification in order to ensure only NGS-compatible amplicon was
521 quantified using the Library Quant ROX Low Kit (Kapa Biosystems) on a QuantStudio™ 6
522 Realtime PCR System (ThermoFisher). Following qPCR quantification, all libraries were
523 normalized to a standard concentration (typically 20-40nM) depending on the lowest
524 concentration library to be pooled, and then requantified by qPCR to ensure all samples were
525 within ~10-20% of the pool mean target concentration. After confirming accurate library
526 quantification and normalization, samples were pooled at an equimolar ratio and submitted for
527 sequencing. Libraries were sequenced on the NovaSeq 6000 instrument (Illumina) (150bp,
528 paired-end) at the University of Colorado Cancer Center Genomics Shared Resource.

529 ***CRISPR screening bioinformatic pipeline and analysis***

530 sgRNA counts were extracted directly from R1 raw sequence reads using a custom perl script
531 that uses regular expression string matching to exactly match sgRNA sequence flanked by 10
532 bases of vector sequence. The vector sequence was allowed to have one error before and after
533 the sgRNA sequence. sgRNAs were tabulated for each sample based on the sgRNA sequence
534 (**Table S15**). The sgRNA IDs of the Brunello library were updated to current HGNC gene names
535 using the Total Approved Symbols download from HGNC, accessed on 9/1/2020
536 (https://www.genenames.org/download/statistics-and-files/). Transcript IDs were matched when
537 possible and when matches were not found, past symbols and aliases were updated to current
538 names. Finally, 5 sgRNAs with missing updated gene names were manually curated using
539 literature searches. Library distribution was calculated using the caRpools R package (47). The
540 DESeq2 R package (48) was used to calculate differential abundance of genes (**Table S5**).
541 Gene counts were generated using the sum of counts for sgRNAs of the same gene. Synthetic
542 lethality compared GemCis day 19 and GemCis day 25 vs. PBS day 19 and PBS day 25 with
543 the day as a covariate. In the comparison integrating all cell lines, cell line was additionally
544 modeled as a covariate. Gene essentiality was calculated by comparing PBS day 25 to PBS day
545 0 and in the integrated all cell lines comparison; cell line was modeled as a covariate. Common
546 synthetic lethal genes were defined as being statistically significantly differentially lost (FDR <
547 0.05 and Log2 FC < 0) in each of the 5 cell lines. Gene set enrichment analysis (GSEA) was
548 performed using the fgsea R package run with 10000 permutations (22) with the KEGG and
549 Reactome gene sets from MSigDB (23). Heatmaps were generated with the ComplexHeatmap
550 R package following z-score transformation (25). Other plots were generated using the ggplot2
551 R package.

552 **Xenograft experiment**

553 Six-week-old, female NU/J mice (Jackson Labs) were allowed to acclimate for at least one week
554 prior to initiating any experiments. Mice had free access to food and water in pathogen-free
555 housing and cared for in accordance NIH guidelines and all experiments were performed under
556 protocols approved by the University of Colorado Denver Institutional Animal Care and Use
557 Committee (IACUC).

558 For KU1919-GC xenografts, cells that had been stably transduced with non-targeting control
559 (shCtrl1, SHC002) and NPEPPS (shN39, TRCN0000073839) shRNA constructs. Mice were
560 divided into groups of 22 and 23 for the non-targeting control and NPEPPS shRNA constructs
561 respectively. Mice were injected with 4e6 cells in phenol red- and serum-free RPMI mixed with
562 equal volume Matrigel Matrix (Corning) to total 100μl volume. Tumors were allowed to engraft
563 for 9 days following injection and mice were randomized based on tumor volume within each
564 shRNA condition into groups of 11 or 12 to be treated with combination gemcitabine plus
565 cisplatin or DPBS. Treatment was initiated 13 days post-inoculation with dosing adjusted based
566 on individual mouse weight.

567 Cisplatin (Sigma) and gemcitabine hydrochloride (BOC Sciences) were both resuspended in
568 0.9% PBS and stored protected from light at -80°C as individual aliquots. Prior to treatment
569 fresh aliquots of gemcitabine and cisplatin were thawed and diluted to their final concentration
570 with 1X DPBS (Gibco). Mice were treated three times weekly on a Monday, Wednesday and
571 Friday schedule for four weeks total. All mice in the gemcitabine plus cisplatin-treated groups
572 were given 50mg/kg gemcitabine and 2mg/kg cisplatin that were mixed and administered as a
573 single intraperitoneal injection, while control mice were administered an equivalent volume of
574 DPBS.

575 Mouse health was monitored daily and all tumor volume measurements and weights were
576 measured 3x weekly schedule. Tumor volume was calculated using the formula (L x W^2)/2, for
577 which *L is* the length of the long axis and *W* is the width of the axis perpendicular to the long
578 axis measurement. All measurements were performed using digital calipers. Animals were
579 humanely euthanized with CO_2 followed by cervical dislocation when tumors reached a
580 predetermined endpoint of $2cm^3$ or when weight loss exceeded 15% body weight. Mice that
581 were removed from the study due to weight loss were censored in the survival analyses.

582

583 **Linear mixed-effects model of tumor growth**

584 Linear mixed-effects models were used to model longitudinal observations of xenograft tumor
585 growth volumes normalized by their corresponding baseline volume. Mixed-effects models from
586 the R-package *lme4* (49) and Satterthwaite's approximation for degrees of freedom for the fixed
587 effects from *lmerTest* (50) were used for model fitting and inspection in the R statistical software
588 (4.0.3). Volume changes compared to baseline were log_2-transformed. The final model was
589 structured as:

590 $$log_2\left(\frac{y_{i,t}}{y_{i,:}}\right) = \beta_0 + \beta_1 x_{i,t} + \beta_2 x_{i,t}^2 + \beta_3 x_{i,t} KD_i + \beta_4 x_{i,t} GC_i + \beta_5 x_{i,t} KD_i\, GC_i + \gamma_{0,i} + \gamma_{1,i} x_{i,t} + \varepsilon_{i,t}$$

591 where β is the fixed effects capturing population-level trends, γ is the normally distributed
592 random effects capturing individual-level variation, ε is the i.i.d. normally distributed residual
593 term, i is the unique individual identifier, t notes the time points, $x_{i,t} \in$
594 $\{2, 4, 5, 7, 9, 11, 14, 16, 18, 21, 23, 25, 28\}$ depicted days since initiating interventions, $y_{i,:}$ is tumor
595 volume at baseline prior to treatments upon randomization, and $y_{i,t}$ were the observed tumor
596 volumes over the treatment period measured in mm^3. The model was fit using Restricted
597 Maximum Likelihood and built iteratively until the underlying model assumptions and model

598 convergence criteria were met. To this end, a quadratic growth term (β_2) was added on top of
599 the linear growth term (β_1) and intercept (β_0), allowing slightly non-linear relative growth patterns
600 to be captured by the otherwise linear model. Binary indicators $KD_i \in \{0,1\}$ and $GC_i \in \{0,1\}$ were
601 used to model knockdown of NPEPPS, GemCis treatment, or the combination. The
602 corresponding model terms were captured in β_3, β_4 and β_5, respectively. Finally, the model
603 allows for individual-specific random effects for intercept ($\gamma_{0,i}$) and linear growth slope ($\gamma_{1,i}$).
604 Shapiro-Wilk test was used to examine the underlying normality assumption for $\gamma_{0,i}$ and $\gamma_{1,i}$ with
605 *p*=0.1373 and *p*=8901, respectively, indicating that these random effects followed underlying
606 assumptions of normality. After inspection of the residual plots (**Figure S7B**), this final model
607 was deemed suitable for population-level statistical inference via the fixed effects. This
608 population-level model fits are visualized in **Figure S7A**. These population-level estimates are
609 as follows:
610

Fixed effect	Estimate	Std. error	df	t	*p*-val
β_0 (intercept)	0.05054	0.08422	54.28	0.600	0.55091
β_1 (linear slope)	0.1236	0.01493	65.52	8.276	8.92e-12 ***
β_2 (quadratic slope)	0.00308	0.0002242	389	13.740	< 2e-16 ***
β_3 (knockdown)	-0.0605	0.01821	44.97	-3.322	0.00178 **
β_4 (GC)	-0.1063	0.01821	44.97	-5.837	5.49e-07 ***
β_5 (knockdown + GC)	-0.1233	0.01791	45.28	-6.884	1.47e-08 ***

611

612 **Patient tumor-derived organoids (PDOs)**

613 ***Culture of the PDOs***

614 Human bladder tissue was obtained from the Erasmus MC Bladder Cancer Center, Rotterdam,
615 the Netherlands and the Amphia Ziekenhuis, Breda, the Netherlands. Bladder tumor-derived
616 organoids from biopsies obtained through TURBT or cystectomy were isolated and cultured
617 using methods developed by Mullenders et al. (51) with modifications (Akbarzadeh/Scholtes et
618 al. in prep). Briefly, bladder tissues were washed with Advanced DMEM/F12 (Gibco)
619 supplemented with 10mM HEPES (Gibco), 1% GlutaMax (Gibco) and 100 µg/ml primocin
620 (InvivoGen), henceforth Ad+++. Tissue was minced and incubated at 37°C with the digestion
621 solution (collagenase 2.5mg/ml in EBSS) and isolated cells were passed through 70µM strainer
622 (Falcon), washed with Ad+++ and seeded in 50 µl drops of BME (R&D system) containing
623 10000-15000 cells in 24 well suspension plates (Greiner). Bladder tumor organoids were
624 cultured in a culture medium containing Ad+++ supplemented with 1 × B-27 (Gibco), 1.25 mM
625 N-acetylcysteine (Sigma), 10 mM nicotinamide, 20µM TGFβ receptor inhibitor A83-01, 100ng/ml
626 recombinant human FGF10 (Peprotech), 25 ng/ml recombinant human FGF7 (Peprotech), 12.5
627 ng/ml recombinant human FGF2 (Peprotech), 10µM Y27632 Rho Kinase (ROCK) Inhibitor
628 (Sigma) and conditioned media for recombinant Rspondin (2.5% v/v), and Wnt3A (2.5% v/v).
629 The medium was changed every three days. Organoids were passaged at a 1:3 to 1:6 ratio
630 every 7 days using cell dissociation solution- non enzymatic (Sigma) and plated in fresh BME
631 matrix droplets.
632

633 ***Lentiviral transduction of bladder cancer PDOs***
634 Lentiviral vectors containing the desired shRNA sequences were amplified from bacterial
635 glycerol stocks obtained in house from the Erasmus Center for Biomics and part of the
636 MISSION® shRNA library. The same shRNA constructs used for bladder cancer cell lines, and
637 described above, were used for PDOs. For overexpression, pLenti-C-Myc-DDK-P2A-Puro
638 Lentiviral Gene Expression Vectors were acquired from Origene (NPEPPS RC209037L3, empty

639 vector PS100092). For lentiviral particle generation, in total, 5e6 HEK293T cells were plated in a
640 10-cm dish and transfected with 12.5 µg of plasmids mix. In total, 4.5 µg of pCMVΔR8.9
641 (envelope), 2 µg of pCMV-VSV-G (packaging) and 6 µg of shRNA vector were mixed in 500 µl
642 serum-free Opti-MEM and combined with 500 µl Opti-MEM containing 125 µl of 10 mM
643 polyethyleneimine (PEI, Sigma). The resulting 1 ml mixture was added to HEK293T cells after
644 15 min incubation at room temperature. The transfection medium was removed after 12 h and
645 replaced with a fresh RPMI medium. Virus-containing medium was harvested and replaced with
646 fresh medium at 48, and 72 h post-transfection. After each harvest, the collected medium was
647 filtered through a cellulose acetate membrane (0.45 µm pore), viral particles were concentrated
648 by ultracentrifugation at 20.000 rounds per minute for 1 hour at 4 °C with pellets re-suspended
649 and pooled in a final volume of 2mL adv. DMEM for each condition. Medium containing viral
650 particles was used either directly or was stored at −80 °C. For lentiviral transduction of bladder
651 cancer organoid cells, organoids were harvested and dissociated to single cells using cell
652 dissociation solution. For each condition (shRNA control / shRNA NPEPPS / NPEPPS-OE /
653 empty vector), 1 × 106 cells were collected and gently re-suspended in 1mL of concentrated
654 lentivirus. Cell-virus mixture was then divided over two wells of a pre-warmed 24-well plate and
655 subsequently sealed with parafilm. Plates were spinoculated at 600 x g at 25 °C for 1 hour.
656 Parafilm was removed immediately after spinoculation, and plates were incubated for 6-8 hours
657 at 37 ˚C 5% CO2. Transduced cells were washed 1 time with 10mL advanced DMEM spinning
658 down at 200 x g for 10 minutes and seeded in domes at a density of 150 cells per µL BME.
659 Once matured, organoids were treated with 2 µg/ml puromycin for 72 hours. Puromycin-selected
660 organoids were then passaged and given 6 days of recovery time prior to experimental
661 procedures.
662

663 ***Ex vivo drug testing***

664 Organoids were collected 4-7 days after passaging and dissociated to single cells using a cell
665 dissociation solution, assisted by mechanical dissociation. All assays were performed in 96 well
666 suspension plates (Greiner bio-one; 655 185), seeding 10,000 cells per well in 100 µl bladder
667 organoid medium containing 15% BME. Drugs were added when mature organoids formed after
668 two-three days, and drug treatment was performed in triplicate. For *ex vivo* cisplatin response:
669 cisplatin (Sigma; PHR1624; reconstituted in NaCl) was added in six doses in the range of 0.1 to
670 40 µM. Caspase-3 and -7 activity was measured following three days of treatment (Caspase-
671 Glo #G8093, Promega), while cell viability was obtained after six days of treatment (CellTiter-
672 Glo 3D #G9681). Plates were read on a SpectraMax I3 plate reader. Viability data was
673 normalized using organoid wells treated with vehicle control (1.2% PBS) (Medchemexpress;
674 HY-14807; reconstituted in DMSO). Organoids were harvested after six days of treatment and
675 dissociated into single cells using a cell dissociation solution, assisted by mechanical
676 dissociation. Three-quarters of the cells were used to obtain cell viability as previously described
677 (treatment), while one-quarter of the cells were reseeded in 200µL BOM + 15% BME. Following
678 reseeding, organoids were allowed to regrow for another six days after which cell viability
679 (reseeding) was again obtained. Cell viability was normalized using organoids treated with
680 vehicle control (0.02% DMSO, 1.2% PBS).

681 ***SNaPshot mutation analysis***

682 Tumor and matched organoid DNA was isolated using with the QIAmp DNA Mini-Kit (Qiagen)
683 according to the manufacturer's protocol. Presence of hotspot mutations in the *TERT* promoter
684 sequence chr5:1,295,228C>T, chr5:1,295,248G>A and chr5:1,295,250C>T [GRCh37/hg19]),
685 *FGFR3* (R248Q/E, S249C, G372C, Y375C, A393E, K652E/M) and *PIK3CA* (E542K, E545G/K
686 and H1047R) were assessed on tumor and organoid DNA by SNaPshot mutation analysis with

687 the same methods as previously described (52–54).
688

689 ***Organoid phenotyping and tumor histology***

690 Tissue processing and H&E staining were performed using standard procedures. For
691 hematoxylin-eosin (H&E) staining of organoids, wells of BME-embedded organoids were fixated
692 with 4% formalin (Sigma) and 0.15% glutaraldehyde (produced in-house) at room temperature
693 for 2 hours. Fixated BME and organoids were washed with PBS and engulfed in 2.5% Low-
694 Melting Agarose (Sigma) prior to paraffin embedding. H&E staining was performed on 4µM
695 paraffin sections of both tumor and organoid tissue. Stained whole-slides, as well as prior 3D
696 organoid cultures, were imaged by bright-field microscopy (Olympus IX70).

697

698 ***Data availability***

699 The mass spectrometry proteomics data have been deposited to the ProteomeXchange
700 Consortium via the PRIDE (55) partner repository with the dataset identifier PXD024742. The
701 whole exome sequencing data have been deposited in the BioProject database with project
702 identifier PRJNA714778. The RNA sequencing data have been deposited in the GEO database
703 with dataset identifier (GSE171537). The CRISPR screen sequencing data have been
704 deposited in the GEO database with dataset identifier (GSE179799). The copy number data
705 have been deposited in the ArrayExpress database with identified (E-MTAB-10353). All data are
706 made available through a custom build R Shiny app at:
707 https://bioinformatics.cuanschutz.edu/BLCA_GC_Omics/
708
709 *Reviewer Login Information*
710 **PRIDE**
711 Username: reviewer_pxd024742@ebi.ac.uk
712 Password: n70lwGNc
713
714 **SRA**
715 https://dataview.ncbi.nlm.nih.gov/object/PRJNA714778?reviewer=50g24ej0558qj2dpr9v6pekgvl
716
717 **GEO (RNAseq)**
718 https://www.ncbi.nlm.nih.gov/geo/query/acc.cgi?acc=GSE171537
719 token: avkdyoiixnettod
720
721 **CRISPR Screen**
722 URL: https://www.ncbi.nlm.nih.gov/geo/query/acc.cgi?acc=GSE179799
723 Reviewer token: elafaomerfarvsr
724
725 **ArrayExpress**
726 Username: Reviewer_E-MTAB-10353
727 Password: u3MpsspP
728
729

RESULTS

We acquired the five human BCa cell lines, KU1919, 5637, T24, TCCSUP, and 253J from the Resistant Cancer Cell Line (RCCL) collection (56,57). For each, we obtained the parental lines (-Par) and derivatives made resistant through dose escalation to cisplatin (-Cis), gemcitabine (-Gem), and the combination of gemcitabine plus cisplatin (-GemCis) (**Figure 1A, Table S1**). We confirmed resistance to the associated drugs for all resistant derivatives in comparison to the parental lines and found them to be consistent with those reported by the RCCL (**Figure S1**) (56,57). These cells represent features and alterations in putative BCa drivers as reported in TCGA (58) and variants reported in ClinVar (59) (**Tables 1**, **S2, S3)**.

Genome-wide CRISPR screens identify 46 common synthetic lethal genes

To study the connection between drug resistance and gene expression, we performed whole-genome loss-of-function screens in each of the five GemCis-resistant cell line derivatives. After transduction of the Brunello CRISPR-Cas9 knockout library (44), we passaged the cells for 10 days to clear essential genes, then split them into phosphate-buffered saline (PBS) or gemcitabine plus cisplatin treatment groups (**Figure 1A**). Each screen was performed at a drug concentration that allowed the GemCis-resistant cells to grow unrestricted, but significantly inhibited the growth of the parental lines (**Table S1**). Screening parameters for each cell line are reported in **Table S4**. We counted sgRNAs 9 and 15 days after the start of treatment (19 and 25 days after transduction). As expected, similar experimental conditions clustered together when correlations were measured across treatment conditions and cell lines (**Figure S2**).

We defined genes as “synthetic lethal” with gemcitabine plus cisplatin treatment as those for which the combined cognate sgRNA counts were significantly lower (moderated t-test, FDR < 0.05) in the gemcitabine plus cisplatin-treated arm compared to the PBS arm when including both days 19 and 25 in the statistical model (**Table S5**). We identified 235 synthetic lethal genes that were statistically significant in KU1919-GemCis, 888 for T24-GemCis, 2099 for TCCSUP-GemCis, 2369 for 253J-GemCis, and 511 for 5637-GemCis. Next, we performed gene set enrichment analysis (60) on the full ranked list of genes according to their synthetic lethality. For this analysis, we created one ranked gene list by including each of the five cell types in the statistical model directly. As expected, and as a validation of the screen itself, we found that the top-ranked pathways were dominated by processes such as DNA repair, Fanconi Anemia, nucleotide excision repair, double-stranded break repair, base-excision repair, and DNA damage bypass mechanisms (**Figure 1B, Table S6**). These results are consistent with the known roles of DNA damage detection and repair in cisplatin resistance (61,62). In addition, the overall ranking of genes from our CRISPR screen showed enrichment for manually curated genes associated with platinum resistance in cancer (63) (**Table S5**).

From these results, we identified 46 genes that were commonly synthetic lethal across all five cell lines (**Figure 1C, S3)**. Consistent with the overall findings (**Figure 1B**), 41 of the 46 common synthetic lethal genes fell into one or more putative DNA damage response and repair pathways, including homologous recombination, double-stranded break repair, nuclear excision repair, and Fanconi anemia (**Figure S3B**, **Table S7**). These genes showed a range of growth patterns over the full length of the CRISPR screen. As illustrated in **Figure 1D**, some genes showed patterns of increased cell growth in PBS treatment, then reduced growth in gemcitabine plus cisplatin treatment. Other genes had very little impact on cell growth in PBS treatment, but then reduced growth when treated with gemcitabine plus cisplatin. Finally, some genes reduced cell growth in PBS treatment and further reduced growth with gemcitabine plus cisplatin

treatment. Overall, these results provide a robust list of known and novel genes involved in chemotherapy resistance that can potentially be targeted therapeutically to improve treatment response.

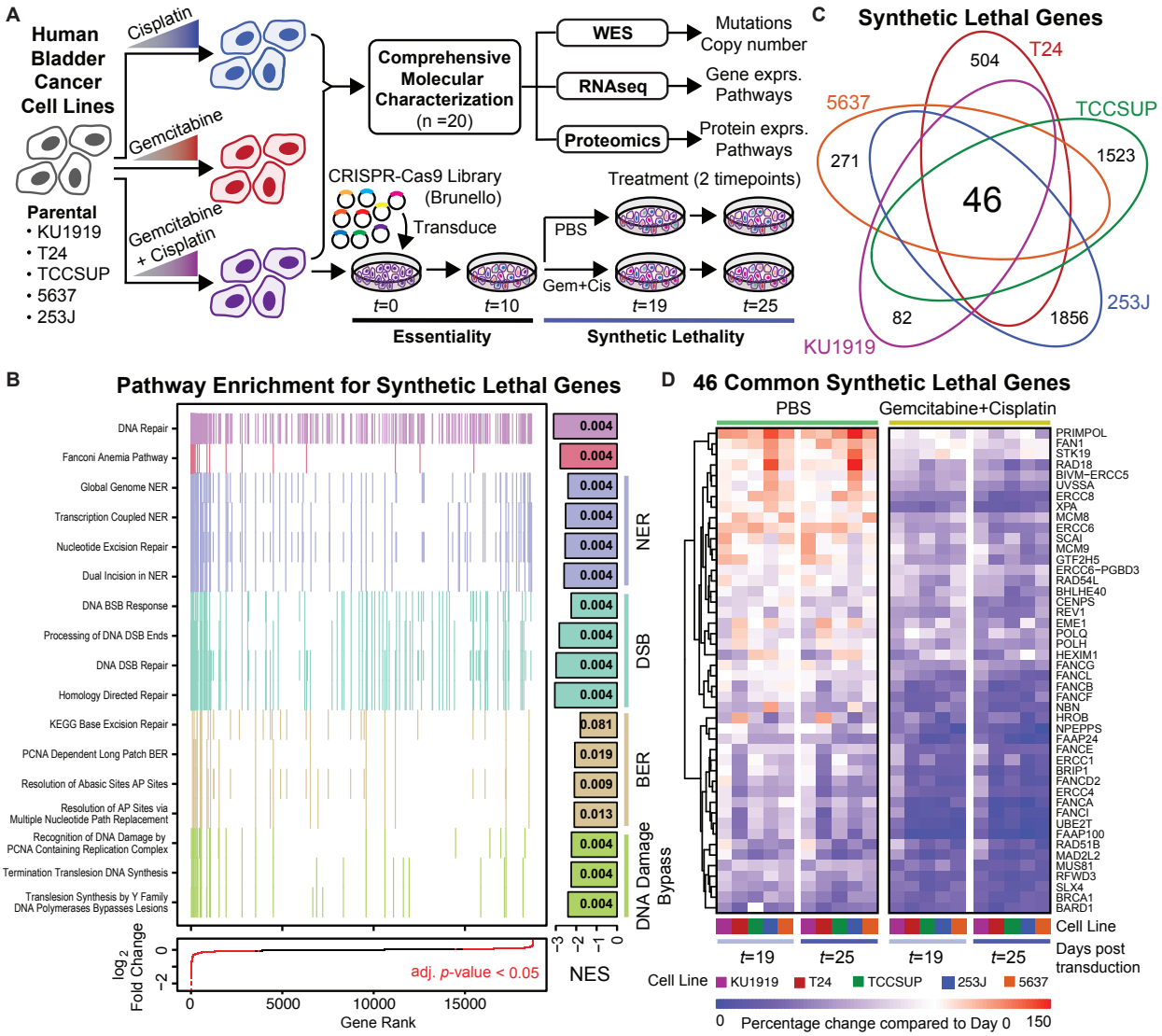

Figure 1. Project overview and synthetic lethal screen results. (**A**) Human bladder cancer cell lines were made resistant to cisplatin, gemcitabine, or gemcitabine plus cisplatin through dose escalation. All cell lines were profiled using -omic technologies. The gemcitabine plus cisplatin-resistant cells were subjected to a pooled CRISPR screen to identify synthetic lethal gene-to-drug relationships. (**B**) Aggregate gene set enrichment results for the synthetic lethal screen ranked by $\log_2$ fold change across all cell lines reveal DNA damage response and repair pathways. Each tick mark represents a gene in the associated pathway. The bars at the right are normalized enrichment scores (NES) with the FDR corrected p-values reported in the bars. (**C**) The intersection across the CRISPR screen results identified 46 common synthetic lethal genes; all counts and gene annotations are reported in **Figure S2**. (**D**) The percentage change in the aggregate of the sgRNAs targeting the 46 commonly synthetic lethal genes are reported across phosphate-buffered saline (PBS) or gemcitabine plus cisplatin treatment arms of the CRISPR screen. Cell lines are coded with the same colors throughout all figures.

Feature	KU1919	T24	TCCSUP	5637	253J
Sex	Male	Female	Female	Male	Male
Stage	T3	Ta	N/A	N/A	T4
Grade	G3	G3	G4	G2	G4
Base47 Subtype	N/A	Basal	Basal	Luminal	Basal
TP53		Y126X	E349X		
HRAS		G12V			
NRAS	Q61R				
PIK3CA			E545K		E545G
TERT					
ARID1A	Y1052X				
KMT2D	T2441Pfs*44			Q2813X	
KDM6A	Q915X				
FAT1		S2682X	D1536N		
KMT2C		R4225X; A3559T			
ERBB2				S310F	
ERBB3		E1219K			
EP300		C1201Y			
FBXW7			S66X		
ASXL2			E330Q		
ATM				H1876Q	
AKT1	E17K				
RYR2		R2401H			
NFE2L2					G81S
RB1			LOSS	Y325X	
E2F3			AMP	AMP	
PPARG				AMP	
CCND1	AMP				
CDKN2A	LOSS				LOSS

798 **Table 1.** Clinicopathologic characteristics and genetic drivers for five cell lines.

799 **Complementary multi-omic profiling prioritizes NPEPPS as the top driver of**
800 **treatment resistance.**
801
802 Pre-treatment multi-omic profiling has been shown to reveal the biological impact of synthetic
803 lethal hits (64). Accordingly, we performed RNA sequencing and mass spectrometry-based
804 proteomic profiling on cell lysates of all cell lines grown in drug-free media (**Figure 1A**). We
805 leveraged transcriptome and proteome profiles from parental to matched drug-resistant
806 derivative lines (-Gem, -Cis, and -GemCis) to prioritize the 46 common synthetic lethal genes
807 that drive resistance in the context of gemcitabine plus cisplatin treatment resistance.
808
809 Taking this approach, the transcriptomics data revealed 1557 significantly upregulated genes
810 across the Gem-resistant lines, 1897 in the Cis-resistant lines, and 1530 in the GemCis-
811 resistant lines (moderated t-test, FDR < 0.05; **Table S9**). The proteomics data revealed 9
812 significantly upregulated proteins across the Gem-resistant cell lines, 1 in the Cis-resistant cell
813 lines, and 10 in the GemCis-resistant cell lines (moderated t-test, FDR < 0.25; **Table S10**).
814 Given the lower number of significant proteins and the relevance of transcript expression in
815 predicting genetic dependency (64), we first investigated the overlap between the CRISPR
816 screen results and the transcriptomes from each of the resistant cell line derivatives compared
817 to the parental cells. Few genes were significantly and consistently upregulated across the
818 resistant derivatives in the list of 46 commonly synthetic lethal genes (**Figure 2A**), but the most
819 significantly and consistently upregulated genes were involved in DNA damage response and
820 repair mechanisms, including ERCC6, XPA, REV1, POLH, ERRC8, PRIMPOL, NBN, and
821 members of the Fanconi Anemia pathway. We identified Puromycin-Sensitive Aminopeptidase,
822 NPEPPS, to be the most consistently upregulated gene across the resistant derivatives at the
823 RNA level (**Figure 2A,B**). Similarly, we found NPEPPS to be consistently and significantly
824 upregulated at the protein level (**Figure 2C**). NPEPPS was also a top synthetic lethal hit (**Figure**
825 **2D, Table S5**). Consistent with the proteomics results, immunoblotting for NPEPPS revealed
826 that it was upregulated in the Cis-resistant and GemCis-resistant lines, with the Gem-resistant
827 lines showing variable upregulation (**Figure 2E**).
828

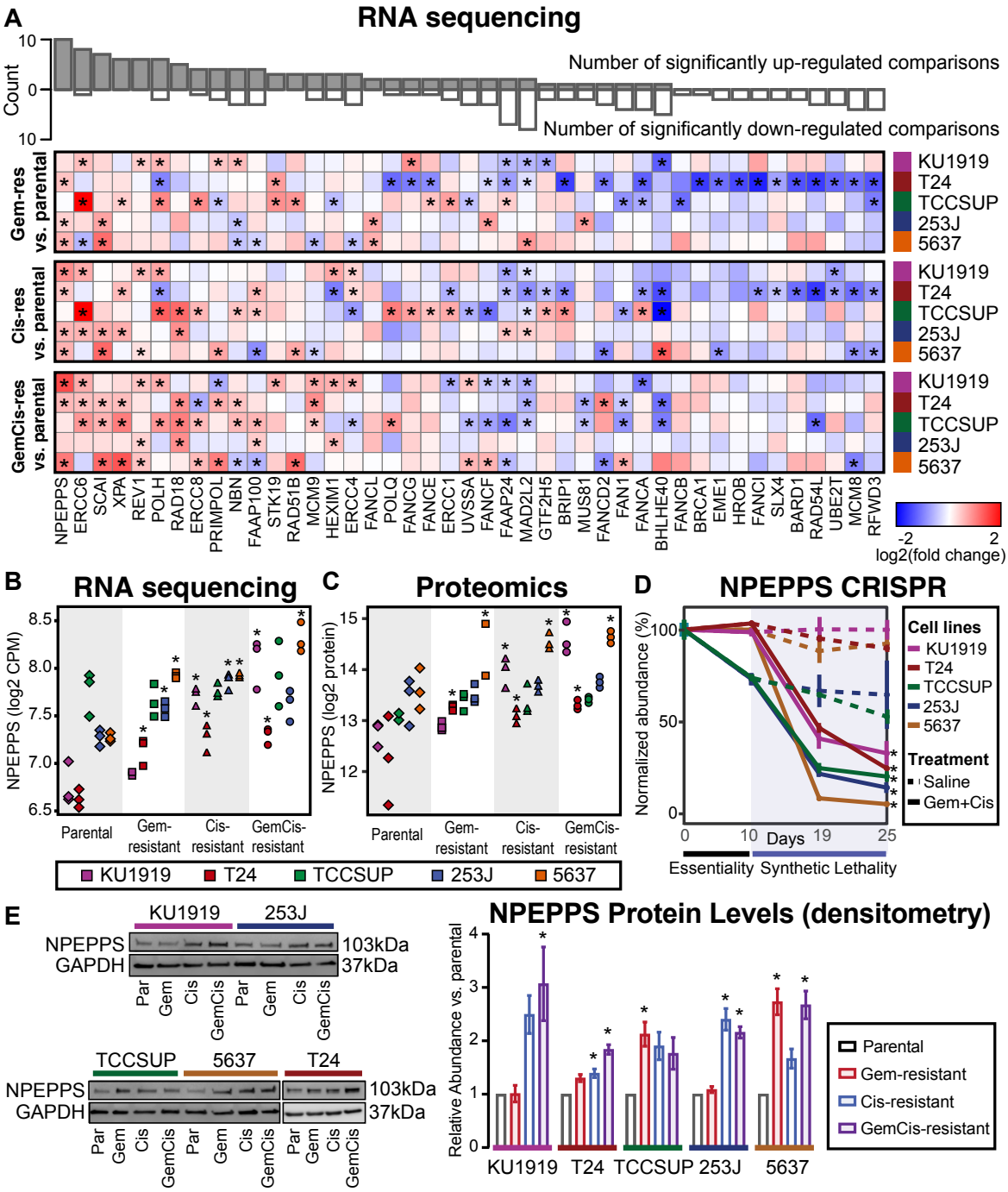

Figure 2. NPEPPS is identified as a commonly upregulated and synthetic lethal hit. (**A**) Differential gene expression of 43 common synthetic lethal genes as measured by RNAseq across all cell lines (43 of 46 genes mapped between RNAseq and the CRISPR screen), comparing the treatment-resistant derivative (Gem-, Cis-, GemCis-resistant) to the associated parental cell line. Asterisks indicate a statistically significant result (moderated t-test, *FDR < 0.05). The bar plot on top is the aggregate count of significant results across all 15 comparisons. Genes are ranked by the count of statistically significant upregulated hits. (**B**) RNAseq (moderated t-test compared to parentals; *FDR < 0.05), (**C**) mass spectrometry proteomics (moderated t-test compared to parentals, *FDR < 0.25), and (**D**) CRISPR screen results for NPEPPS (mean ± SD; moderated t-test; *FDR < 0.05). (**E**) Representative immunoblots and densitometry quantification for independent triplicates (mean ± SEM) for NPEPPS in all cell lines (*FDR < 0.05).

841 **NPEPPS drives cisplatin resistance *in vitro* and *in vivo***
842
843 To test our prioritization that NPEPPS regulates sensitivity to gemcitabine plus cisplatin
844 treatment in GemCis-resistant BCa cells, and to parse its role in both cisplatin and gemcitabine
845 resistance, we generated stable NPEPPS shRNA knockdowns in the KU1919-GemCis and T24-
846 GemCis cell lines. We found that NPEPPS knockdown preferentially increased cisplatin, but not
847 gemcitabine sensitivity (**Figure 3A, C**). Knockdown of NPEPPS did delay the growth of cells but
848 did not have major effects on cell growth rates (**Figure S4A**). siRNA targeting of NPEPPS in the
849 KU1919-GemCis cell line and shRNA and/or siRNA in T24-GemCis and 253J-GemCis cells
850 confirmed our results that NPEPPS loss preferentially sensitizes cells to cisplatin (**Figure**
851 **S4B,C**). Additionally, we used a gRNA from the CRISPR screen library to show that knockout of
852 NPEPPS and the associated dose response matches our findings from shRNA and siRNA-
853 mediated depletion of NPEPPS (**Figure S4D**). Conversely, overexpression of NPEPPS in
854 KU1919 and T24 parental lines increased resistance to cisplatin, but not gemcitabine (**Figure**
855 **3B,D**). These results support NPEPPS as a regulator of sensitivity to gemcitabine plus cisplatin
856 through its effect on regulating the cellular response to cisplatin.
857
858 To evaluate NPEPPS impact on intracellular cisplatin concentrations, we directly measured
859 intracellular cisplatin using the metal ion detection capabilities of cytometry by time-of-flight,
860 CyTOF (65). We measured intracellular cisplatin after 4 hours of treatment at 10μM in the same
861 KU1919 and T24 cells evaluated for dose response. Using KU1919 as the illustrative example,
862 KU1919-GemCis cells (median Pt 195 = 102) showed lower cisplatin concentration compared to
863 KU1919 parental cells (median Pt 195 = 565). Control knockdown had little effect (median Pt
864 195 = 121), but NPEPPS knockdown shifted the intracellular levels of cisplatin to the parent
865 lines (median Pt 195 = 375), suggesting that NPEPPS depletion increased intracellular cisplatin
866 (**Figure 3E** and **S5**). These findings were replicated in the T24 cell lines (**Figure 3E** and **S5**)**.** In
867 the overexpression setting, and using KU1919 as the example, KU1919-GemCis cells (median
868 Pt 195 = 763) again showed lower cisplatin concentration compared to KU1919 parental cells
869 (median Pt 195 = 1706) with the overexpression control cells (median Pt 195 = 1738) showing
870 little difference, but the NPEPPS overexpressing cells (median Pt 195 = 1203) showing a
871 decrease in intracellular cisplatin (**Figure 3F** and **S6**). We found similar results with T24 cells
872 (**Figure 3F** and **S6**). These data are consistent with the dose response results reported in
873 **Figure 3A-D**.
874
875 To test if NPEPPS depletion sensitizes tumor cells to cisplatin-based chemotherapy *in vivo*, we
876 established subcutaneous xenografts using the KU1919-GemCis cells with either NPEPPS
877 shRNA knockdown or non-targeting shRNA control. When tumors reached roughly 200mm^3,
878 mice were randomized into four groups: shCtrl1 with PBS (n=11), shCtrl1 with gemcitabine plus
879 cisplatin (n=11), shN39 with PBS (n=11), and shN39 with gemcitabine plus cisplatin (n=12).
880 Treatment was delivered through intraperitoneal injection, with PBS or gemcitabine plus
881 cisplatin administered three times weekly for four weeks. Tumor volumes were monitored until
882 they reached the predetermined endpoint of 2cm^3. NPEPPS knockdown alone and gemcitabine
883 plus cisplatin treatment alone had a significant impact on tumor growth compared to vehicle-
884 treated, shRNA controls. The combination of NPEPPS knockdown and gemcitabine plus
885 cisplatin treatment led to a stronger and more significant impact on tumor growth (**Figure 3G**).
886 We further analyzed tumor growth using linear mixed-effects models aimed at capturing trends
887 in tumor volume change in relation to pre-treatment baseline tumor volume across the four
888 groups (**Figure S7A,B**). According to this model, tumor growth inhibition by NPEPPS
889 knockdown (p=0.00178), GemCis treatment (p=5.49e-7), or the combination of NPEPPS
890 knockdown and gemcitabine plus cisplatin treatment (p=1.47e-8) were all consistent effects
891 over the treatment period (**Figure 3G,H**). We validated NPEPPS knockdown in the pre-

xenograft inoculate cells and after tumors were removed from mice upon reaching the $2cm^3$ endpoint (**Figure S7C**). Survival analysis using tumor volume as the endpoint showed that mice treated with gemcitabine plus cisplatin had a 14-day survival advantage. Similarly, the knockdown of NPEPPS resulted in a 14-day survival advantage. Mice treated with gemcitabine plus cisplatin and with NPEPPS knockdown tumors had a 25-day survival advantage, a statistically significant improvement (Logrank test, p<0.0001) (**Figure 3H**).

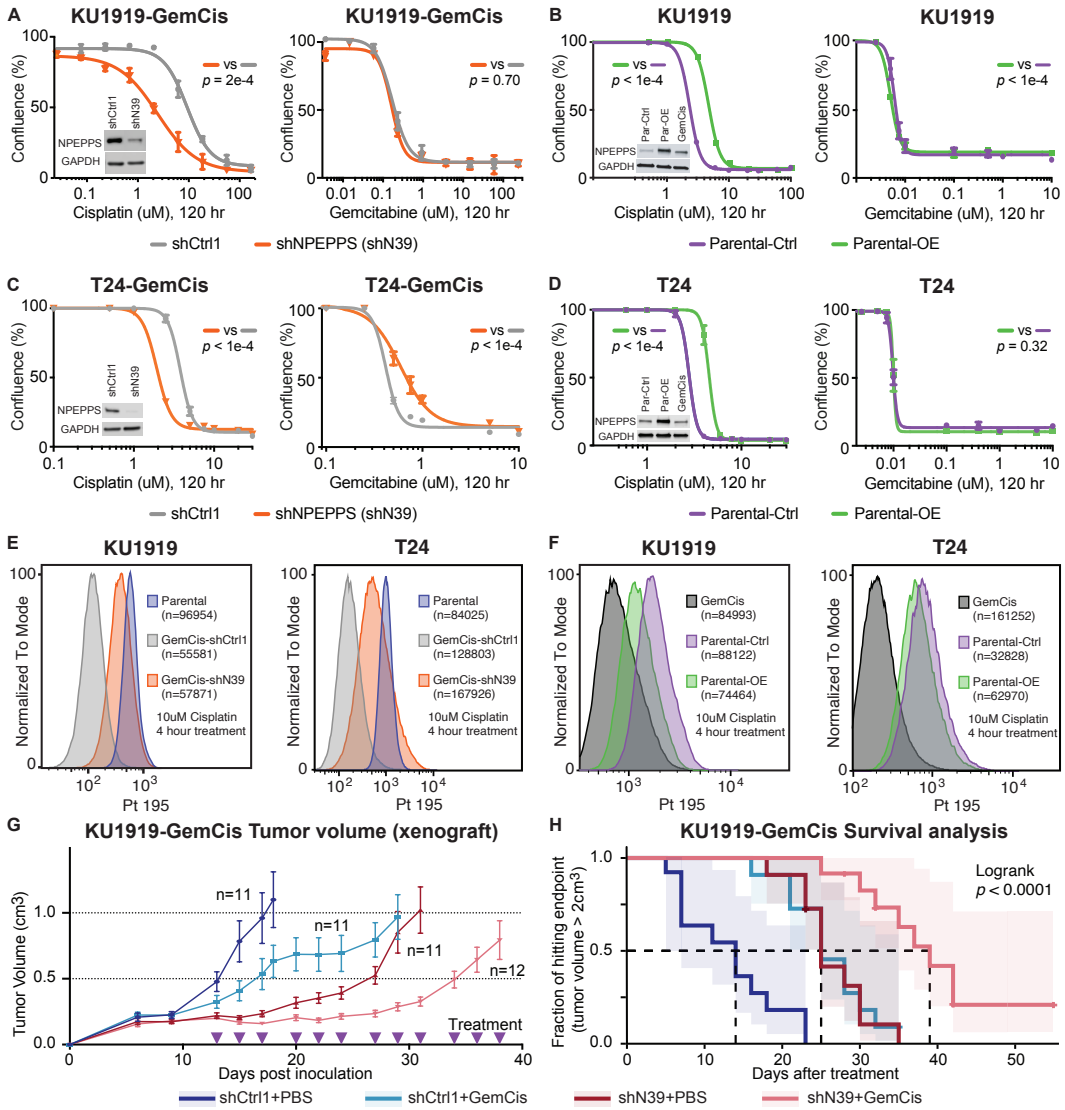

Figure 3. Genetic inhibition of NPEPPS resensitizes GemCis-resistant cells *in vitro* and *in vivo*. (**A, B**) KU1919-GemCis or T24-GemCis cells with knockdown of NPEPPS treated with increasing doses of cisplatin or gemcitabine. A total of 3 technical replicates per dose (mean ± SEM). (**C**, **D**). KU1919 or T24 parental cells with overexpression of NPEPPS treated with increasing doses of cisplatin or gemcitabine. A total of 3 technical replicates per dose (mean ± SEM). Independent experiments are reported in **Figure S4**. p-values comparing IC50 values using sum-of-squares F test. (**E,F**) Intracellular cisplatin levels in KU1919 T24 cells were measured after 4 hours of 10μM cisplatin treatment using CyTOF, with the number of live cells analyzed as indicated. (**G**) Tumor volume (mean ± SEM) of KU1919-GemCis xenografts measured over time and across 4 treatment groups considering non-targeting shRNA controls (shCtrl1), shRNA targeting NPEPPS (shN39), PBS vehicle control (PBS), or gemcitabine plus cisplatin treatment (GemCis). (**H**) Survival analysis of xenograft models with a defined endpoint of a tumor volume > $2cm^3$. Logrank test was applied to test significance.

912 **NPEPPS regulates cisplatin response in MIBC patient-derived organoids**
913
914 We next evaluated the role of NPEPPS in regulating cisplatin response in *ex vivo* expanded 3D
915 primary cultures of MIBC tissue as patient-derived organoids (PDOs). PDOs are commonly
916 used as an intermediate step to the clinical investigation of novel therapeutics as they more
917 closely recapitulate the human tumor as supported by a high degree of clinical reliability and
918 predictability of drug response in validation trials (66–69). As shown in **Figure 4A**, PDOs were
919 generated from MIBC patients undergoing transurethral resection of a bladder tumor (T, n=3) or
920 radical cystectomy (C, n=2). Three PDOs were generated prior to cisplatin-based chemotherapy
921 (preChemo), one PDO was generated after patients received cisplatin-based chemotherapy
922 (postChemo), and one PDO was generated from patients that did not receive cisplatin-based
923 chemotherapy (noChemo). The tumor for patient 4 showed pathological complete response
924 (pCR), while the tumors for the remaining chemotherapy-treated patients were pathological non-
925 responders (pNR).
926
927 The tumor origin of the PDOs was confirmed by the detection of matching bladder cancer-
928 specific mutations in tumor-organoid pairs (**Figure 4A**). As expected with this patient-derived
929 platform, PDOs displayed distinct and tumor-specific phenotypes with notable variations in cell
930 density and roundness (**Figure 4B**). We performed dose response with cisplatin to determine
931 patient-specific *ex vivo* responses. PDOs displayed a range of responses to cisplatin, with a
932 median cisplatin IC50 value of 6.1 μM, a minimum of 2.9 μM, and a maximum of 37.4 μM
933 **(Figure 4C**).
934
935 To investigate the effect of NPEPPS depletion on cisplatin resistance, we selected two PDO
936 lines from patients with clinical neoadjuvant chemotherapy (NAC)-resistance and intermediate
937 *ex vivo* cisplatin resistance (1C-postChemo-pNR and 2T-preChemo-pNR), and performed
938 shRNA-mediated knockdown of NPEPPS (**Figure 4D-E**) followed by their treatment with
939 cisplatin for six days (**Figure 4F,I**). NPEPPS depletion lowered the cisplatin IC50 values by
940 approximately 5μM in both of the tested PDOs (**Figure 4G,J**). Furthermore, significantly
941 increased caspase-3 and -7 activity was observed following three days of cisplatin treatment in
942 shRNA-mediated NPEPPS depletion compared to control PDOs, suggesting that NPEPPS
943 depletion increases cisplatin-mediated apoptosis (**Figure 4H,K)**. Finally, we show that
944 intracellular cisplatin levels in the shRNA control organoids (median Pt 195 = 113) are increased
945 with the knockdown of NPEPPS (median Pt 195 = 213; **Figure 4L**). Collectively, these results
946 demonstrate that genetic inhibition of NPEPPS sensitizes PDOs to cisplatin, which is consistent
947 with our findings in the bladder cancer cell lines.
948
949 Next, we tested whether NPEPPS independently increases cisplatin resistance. We selected
950 treatment-naïve (5C-noChemo) and post-NAC (1C-postChemo-pNR) PDO lines to represent
951 treatment-naïve and cisplatin-treated patients with exogenously expressed NPEPPS via
952 lentiviral transduction (**Figure 5A**). NPEPPS overexpression was confirmed by RT-qPCR,
953 showing a 10-fold overexpression for 5C-noChemo and 3-fold overexpression for 1C-
954 postChemo-pNR (**Figure 5B**). Cisplatin dose response was measured and we observed a
955 decrease in cisplatin-mediated apoptotic blebbing and loss of structure in NPEPPS-
956 overexpressing PDOs compared to empty vector control PDOs (**Figure 5C,G**). Furthermore,
957 from the estimated IC50 values, we observed an increase in resistance to cisplatin associated
958 with increased NPEPPS expression (**Figure 5D,H**). Moreover, less apoptosis was observed in
959 NPEPPS-overexpressed PDOs treated with 15 μM and 25 μM cisplatin, as measured by
960 caspase-3 and -7 (**Figure 5E,I**). Again, we found that NPEPPS controlled intracellular cisplatin
961 concentrations, with the NPEPPS overexpressing cells (median Pt 195 = 682) showing
962 decreased levels of cisplatin compared to the empty vector control cells (median Pt 195 = 996;

963 **Figure 5F**). Taken together, these results suggest that NPEPPS regulates cisplatin response in
964 treatment naïve and post-NAC treatment PDOs, highlighting NPEPPS as an attractive
965 therapeutic target across cisplatin-based chemotherapy settings.
966

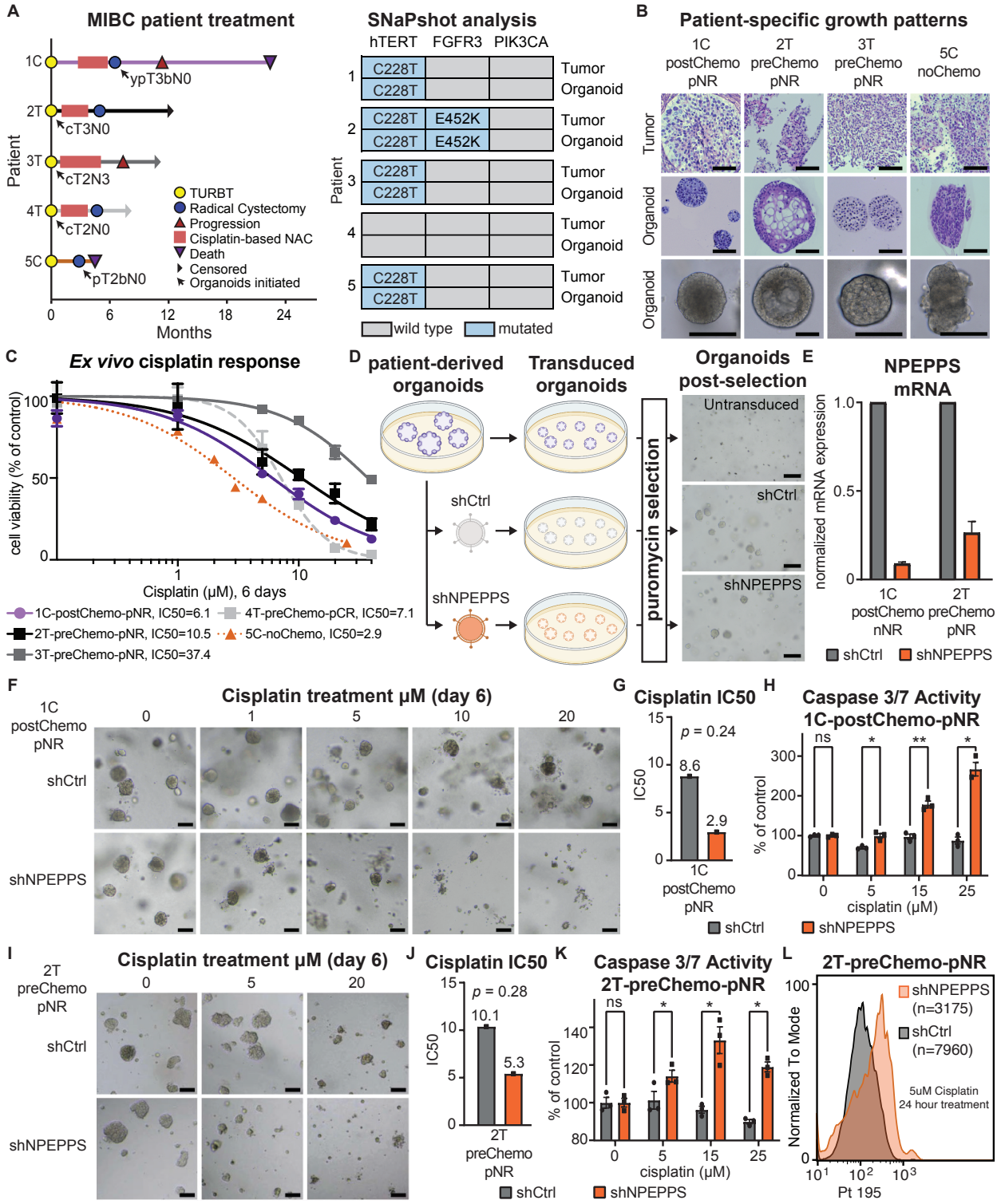

967
968 **Figure 4. NPEPPS depletion sensitizes *ex vivo* models of bladder cancer to cisplatin.** (**A**) Clinical
969 course of muscle-invasive bladder cancer (MIBC) for patients including the point at which the patient

970 tumor-derived organoid lines (PDO) were generated (indicated by the black arrow). Notation is the patient
971 number followed by the tumor source, either T = TURBT = transurethral resection of bladder tumor, or C
972 = radical cystectomy. (**B**) Representative bright-field images of organoids together with H&E staining of
973 patient tumor-PDO pairs illustrating patient-specific growth patterns. Most PDOs exhibited round and
974 dense structures, as represented by 1C-postChemo-pNR (Chemo = cisplatin-based chemotherapy
975 regimen, pNR = pathological non-responder), although there was notable variation in growth and
976 morphology. Scale bar = 100µm. (**C**) *Ex vivo* response of all nine PDOs treated with increasing
977 concentrations of cisplatin. Cell viability, as a percentage of untreated control, was measured using
978 CellTiter-Glo. The fitted dose-response curves represent viability corresponding to three biological
979 replicate experiments and data are represented as mean ± SEM. pCR= pathological complete response.
980 (**D**) Experimental workflow for lentiviral, shRNA-mediated NPEPPS-depletion in PDOs and representative
981 images after puromycin selection. Scale bar = 400µm. (**E**) NPEPPS expression was evaluated by RT-
982 PCR in shNPEPPS and shCtrl PDO lines normalized to cyclophilin. Error bars represent mean ± SD. (**F,I**)
983 Representative bright-field images of control and NPEPPS-depleted PDOs, (**F**) 1C-postChemo-pNR or (**I**)
984 2T-preChemo-pNR,treated with the indicated cisplatin concentrations. Scale bar = 200µm. (**G,J**) IC50
985 values estimated from dose curves for cell viability measured through CellTiter-Glo (biological triplicates;
986 mean ± SEM). (**H,K**) Relative caspase-3 and -7 activity in cisplatin-treated shCtrl and shNPEPPS PDOs.
987 Caspase activity was measured by Caspase-Glo and normalized to untreated PDOs. (biological
988 triplicates; mean ± SEM). (**L**) Intracellular cisplatin levels were measured after 24 hours of 5µM cisplatin
989 treatment using CyTOF, with the number of live cells analyzed as indicated.
990

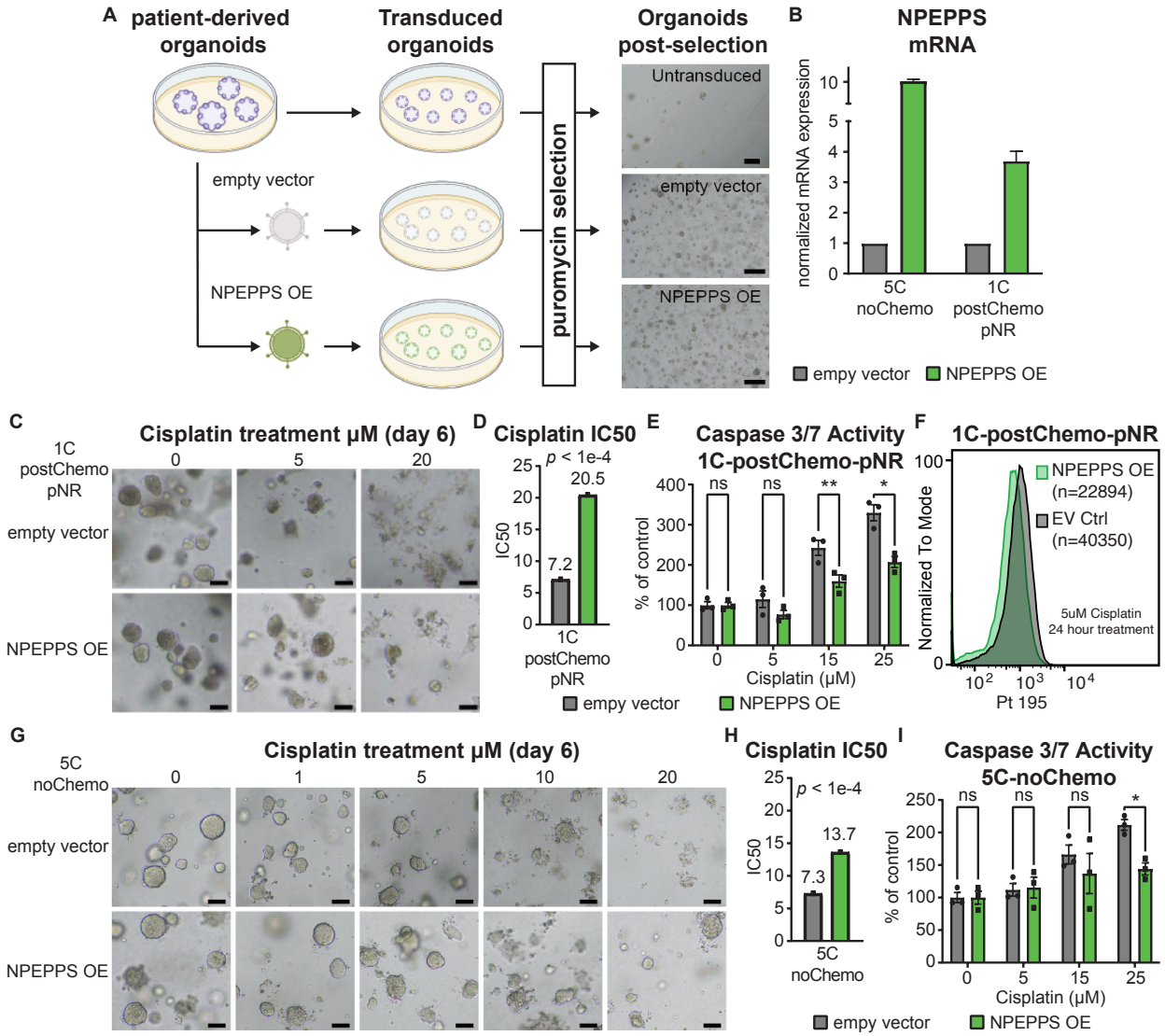

Figure 5. *Ex vivo* NPEPPS overexpression enhances cisplatin resistance. (**A**) Schematic representation of the experimental procedure for NPEPPS overexpression in PDOs and representative images after puromycin selection. Scale bar = 400µm. **B)** NPEPPS expression was evaluated by RT-PCR in shNPEPPS and shCtrl PDO lines normalized to cyclophillin. Error bars represent mean ± SD. (**C,G**) Representative bright-field images of empty vector control and NPEPPS-overexpressing PDOs, (**C**) 1C-postChemo-pNR or (**G**) 5C-noChemo, treated with the indicated cisplatin concentrations. Scale bar = 400µm. (**D,H**) IC50 values estimated from dose curves for cell viability measured through CellTiter-Glo (biological triplicates; mean ± SEM). (**E,I**) Relative caspase-3 and -7 activity in cisplatin-treated empty vector control and NPEPPS-overexpressing PDOs. Caspase activity was measured by Caspase-Glo and normalized to untreated PDOs. (biological triplicates; mean ± SEM). (**F**) Intracellular cisplatin levels were measured after 24 hours of 5µM cisplatin treatment using CyTOF, with the number of livecells analyzed as indicated.

1005 **Pharmacological inhibition of NPEPPS improves cisplatin response in MIBC organoids**
1006
1007 To assess the pharmacological efficacy of targeting NPEPPS, we tested cisplatin treatment
1008 combined with the NPEPPS inhibitor, tosedostat (70). We focused on the three preChemo,
1009 TURBT-derived PDOs to test the efficacy of cisplatin-based chemotherapy in combination with
1010 tosedostat in treatment naïve MIBC patients that will subsequently receive pre-operative
1011 chemotherapy. From our initial evaluation of cisplatin sensitivity (**Figure 4C**), we found the most
1012 sensitive PDO in this group to be 4T-preChemo-pCR (IC50=7.1μM), followed by 2T-preChemo-
1013 pNR (IC50=10.5μM), and the most resistant to be 3T-preChemo-pNR (IC50=37.4μM). This
1014 range of sensitivities matches with the clinical response of patient tumors, where patient 4 had a
1015 pathological complete response (ypT0N0), patient 2 had residual disease following NAC
1016 (ypT3aN0), and patient 3 progressed to metastatic disease during pre-operative chemotherapy
1017 (ypTxNxM+) (**Figure 6A**).
1018
1019 Given that these PDOs are representative molecular (**Figure 4A**), morphological (**Figure 4B**),
1020 and pharmacological (**Figure 4C**) models of patient tumors, we treated the three PDOs with
1021 cisplatin, tosedostat, or the combination of cisplatin plus tosedostat (**Figure 6B**) based on
1022 previously identified plasma concentrations (70–75). Response to 2μM and 5μM cisplatin were
1023 consistent with our previous results (**Figure 4C**), with 4T-preChemo-pCR being the most
1024 sensitive to cisplatin (**Figure 6C, Figure S6A**). Tosedostat alone did not result in significant
1025 changes in viability for the 4T-preChemo-pCR and 2T-preChemo-pNR PDOs, but did result in a
1026 significant reduction in cell viability for 3T-preChemo-pNR, potentially highlighting a role for
1027 tosedostat as a monotherapy in some contexts (**Figure 6C, Figure S6A**). Significant reductions
1028 in cell viability were observed for all PDOs when cisplatin and tosedostat were combined after 6
1029 days of treatment (**Figure 6C**, **Figure S6A**). Importantly, cisplatin response of 4T-preChemo-
1030 pCR was not compromised, but was further enhanced with the addition of tosedostat.
1031
1032 Next, we assessed the ability of drug-treated PDOs to re-establish, which is analogous to a
1033 clonogenic assay, and tests for cellular potential to outgrow following treatment (**Figure 6B,D**).
1034 After reseeding PDOs treated with 5μM cisplatin, 4T-preChemo-pCR showed an absence of
1035 organoid formation or outgrowth, while robust re-growth was observed for PDOs derived from
1036 tumors with residual or progressive disease (2T-preChemo-pNR and 3-preChemo-pNR) (**Figure**
1037 **6D,E, Figure S6B**). Cisplatin plus tosedostat combination treatment eliminated PDO re-growth
1038 for all lines (**Figure 6E**). We additionally tested if tosedostat affected intracellular cisplatin
1039 concentrations similar to NPEPPS depletion. We found that priming bladder cancer cells with
1040 1μM tosedostat for 72 hours followed by 10μM of cisplatin for 4 hours phenocopied NPEPPS
1041 depletion. Intracellular cisplatin in the KU1919-GemCis cells (median Pt 195 = 114) shifted to
1042 the same level as the KU1919-parental (media Pt 195 = 304) when pre-treated with tosedostat
1043 (median Pt 195 = 298). The parental lines also showed increased intracellular cisplatin after
1044 tosedostat pre-treatment (median Pt 195 = 410) (**Figure 3F**). Taken together, these findings
1045 provide strong evidence that tosedostat enhances cisplatin activity in clinically relevant and
1046 translatable experimental models of human bladder cancer, most likely by regulating
1047 intracellular cisplatin concentrations.

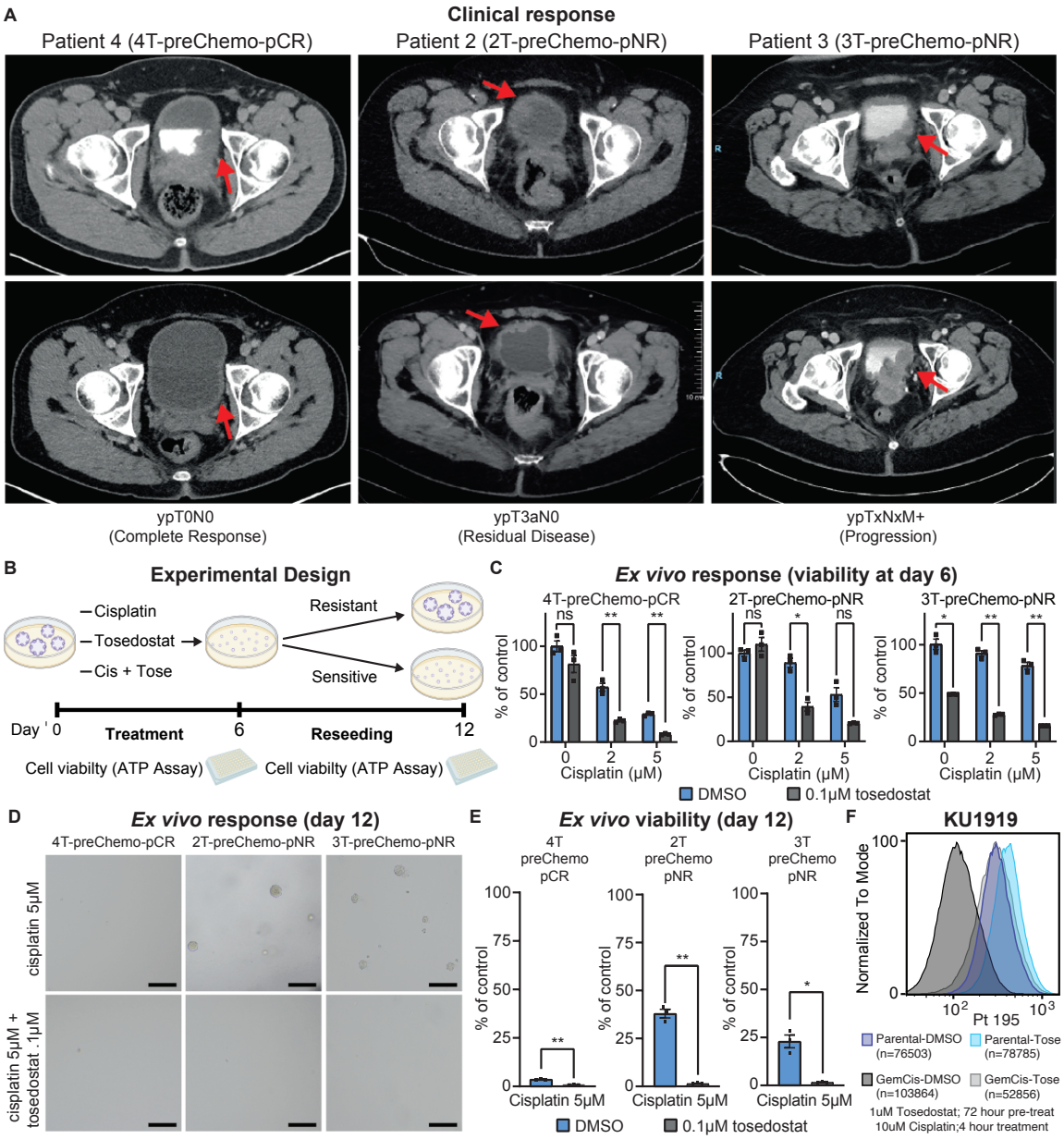

Figure 6. NPEPPS-inhibitor tosedostat overcomes cisplatin resistance ex vivo. (**A**) Clinical response to cisplatin-based chemotherapy in three MIBC patients. Pathological pre-operative chemotherapy response is annotated according to pathological stage following radical cystectomy or metastatic biopsy. Response is illustrated by pre- (top) and post-treatment (bottom) computerized tomography (CT) scans. Red arrows indicate bladder wall thickening and subsequence response. (**B**) Experimental design for treating PDOs with cisplatin and tosedostat alone or in combination. PDOs were withdrawn from treatment, dissociated to single cells and reseeded after 6 days. Cell viability was measured using CellTiter-Glo at day 6 and day 12. (**C**) *Ex vivo* response of PDOs treated with the indicated concentrations of cisplatin with or without the addition of tosedostat. After 6 days viability was measured by CellTiter-Glo. (biological triplicates; mean ± SEM). one-way ANOVA; *P<0.05, **P<0.005. (**D**) Representative bright-field images of reseeded organoids treated with cisplatin or cisplatin + tosedostat as indicated. Scale bar = 400μm. (**E**) Cisplatin response in reseeded organoids treated at the indicated concentrations of drug with viability measured by CellTiter-Glo. (biological triplicates; mean ± SEM). one-way ANOVA; *P<0.05, **P<0.005. (**F**) CyTOF results for KU1919-Parental or -GemCis cells treated with 1μM tosedostat or DMSO for 72 hours, followed by 10μM cisplatin for 4 hours.

1065 **DISCUSSION**
1066
1067 NPEPPS has been suggested to play a role in a range of cellular processes including promoting
1068 autophagy, regulating cell cycle progression, and antigen processing (76–79). The majority of
1069 what is known about NPEPPS has been from studies in the brain, where it targets the
1070 degradation of polyglutamine sequences and misfolded protein aggregates associated with a
1071 number of neurodegenerative diseases, including Alzheimer's disease, Huntington's disease,
1072 and Parkinson's disease (77,80–83). As reported in gnomAD, NPEPPS is a highly conserved
1073 gene and is constrained based on several metrics of intolerance to genetic variation in the
1074 population (84). NPEPPS is also ubiquitously expressed across human tissues (85). However,
1075 despite these features, genetic modification in mice is tolerable, though mice are slower
1076 growing, more sickly, and sterile (79,86), and as we have shown from our CRISPR screen
1077 results and follow-up experiments, knockout is not essential for growth in bladder cancer cells
1078 (**Figure 2D, S4**).
1079
1080 This work is not without its limitations. NPEPPS could have effects on treatment response
1081 outside of platinum drugs. For example, NPEPPS is upregulated in the Gem-resistant cell lines
1082 (**Figure 2**), and while we show that genetic NPEPPS loss is specific to cisplatin response
1083 (**Figure 3, S4**), NPEPPS upregulation could be part of broader cellular stress responses.
1084 Further studies will be needed to test other NPEPPS-mediated mechanisms of stress response.
1085 We note that all of our data support a cell autonomous effect of NPEPPS. As we indicated
1086 above, NPEPPS has been linked to mechanisms of immune response and non-cell autonomous
1087 effects of NEPPS were not tested here. Finally, we show that NPEPPS changes intracellular
1088 platinum drug concentrations. The mechanism by which NPEPPS regulates these intracellular
1089 levels requires future studies.
1090
1091 Despite these limitations, all of our data suggest that NPEPPS is a viable therapeutic target.
1092 Broadly, aminopeptidases have been therapeutically targeted as potential cancer treatments
1093 (87). More specifically, NPEPPS is a zinc-containing M1 aminopeptidase. Tosedostat was
1094 developed as a target of M1 aminopeptidases and the intracellular metabolized product CHR-
1095 79888 is the most potent inhibitor of NPEPPS reported (70,88). There have been a total of 11
1096 clinical trials with tosedostat as reported in *clinicaltrials.gov* (73,74,88–90). The focus of its
1097 application has been in leukemias and myelomas, with several applications in solid tumors. The
1098 few clinical trials completed have reported tosedostat as being well tolerated by patients, but
1099 with modest effect as a single agent cancer treatment. A few examples of tosedostat in
1100 combination with cytarabine, azacitidine, capecitabine or paclitaxel have been tried, but there
1101 are no reports of tosedostat being tested in combination with platinum-based chemotherapy.
1102 This idea can also extend to the many patients that are ineligible for cisplatin-based
1103 chemotherapies by allowing a cisplatin dose reduction in the context of a cisplatin plus
1104 tosedostat combination. Furthermore, future determination of whether NPEPPS inhibition
1105 enhances carboplatin sensitivity may offer these patients an even more effective and less toxic
1106 drug combination option.
1107
1108 In conclusion, our finding that NPEPPS regulates cisplatin-based chemoresistance is both novel
1109 and actionable. Patient tumor-derived organoids (PDOs) have shown predictive value
1110 supporting personalized medicine in several tumor types (66–69,91,92). Our data with PDOs
1111 provides a strong preclinical rationale for the development of clinical trials evaluating tosedostat
1112 in combination with cisplatin (2).

Acknowledgements

We would like to thank Megan Tu, Colin Sempeck, Ana Chauca-Diaz, Jason Duex, and Charles Owens for their help throughout this project. We would also like to thank Dania Manalo-Mae and the Cedars-Sinai Proteomics and Metabolomics Core Facility for the technical handling of the proteomic experiments.

References

1. Dilruba S, Kalayda GV. Platinum-based drugs: past, present and future. Cancer Chemother Pharmacol. 2016;77:1103–24.

2. Rottenberg S, Disler C, Perego P. The rediscovery of platinum-based cancer therapy. Nat Rev Cancer. Nature Publishing Group; 2021;21:37–50.

3. Bray F, Ferlay J, Soerjomataram I, Siegel RL, Torre LA, Jemal A. Global cancer statistics 2018: GLOBOCAN estimates of incidence and mortality worldwide for 36 cancers in 185 countries. CA Cancer J Clin. 2018;68:394–424.

4. Galsky MD, Pal SK, Lin S-W, Ogale S, Zivkovic M, Simpson J, et al. Real-World Effectiveness of Chemotherapy in Elderly Patients With Metastatic Bladder Cancer in the United States. Bladder Cancer Amst Neth. 2018;4:227–38.

5. Galsky MD, Arija JÁA, Bamias A, Davis ID, De Santis M, Kikuchi E, et al. Atezolizumab with or without chemotherapy in metastatic urothelial cancer (IMvigor130): a multicentre, randomised, placebo-controlled phase 3 trial. Lancet Lond Engl. 2020;395:1547–57.

6. Nadal R, Bellmunt J. Management of metastatic bladder cancer. Cancer Treat Rev. 2019;76:10–21.

7. Grossman HB, Natale RB, Tangen CM, Speights VO, Vogelzang NJ, Trump DL, et al. Neoadjuvant Chemotherapy plus Cystectomy Compared with Cystectomy Alone for Locally Advanced Bladder Cancer. N Engl J Med. Massachusetts Medical Society; 2003;349:859–66.

8. Vale CL. Neoadjuvant Chemotherapy in Invasive Bladder Cancer: Update of a Systematic Review and Meta-Analysis of Individual Patient Data: Advanced Bladder Cancer (ABC) Meta-analysis Collaboration. Eur Urol. 2005;48:202–6.

9. Witjes JA, Bruins HM, Cathomas R, Compérat EM, Cowan NC, Gakis G, et al. European Association of Urology Guidelines on Muscle-invasive and Metastatic Bladder Cancer: Summary of the 2020 Guidelines. Eur Urol. 2020;

10. Patel VG, Oh WK, Galsky MD. Treatment of muscle-invasive and advanced bladder cancer in 2020. CA Cancer J Clin. 2020;

1149 11. Cowley GS, Weir BA, Vazquez F, Tamayo P, Scott JA, Rusin S, et al. Parallel genome-scale
1150 loss of function screens in 216 cancer cell lines for the identification of context-specific
1151 genetic dependencies. Sci Data. Nature Publishing Group; 2014;1:140035.

1152 12. McDonald ER, de Weck A, Schlabach MR, Billy E, Mavrakis KJ, Hoffman GR, et al. Project
1153 DRIVE: A Compendium of Cancer Dependencies and Synthetic Lethal Relationships
1154 Uncovered by Large-Scale, Deep RNAi Screening. Cell. 2017;170:577-592.e10.

1155 13. Tsherniak A, Vazquez F, Montgomery PG, Weir BA, Kryukov G, Cowley GS, et al. Defining a
1156 Cancer Dependency Map. Cell. Elsevier; 2017;170:564-576.e16.

1157 14. Behan FM, Iorio F, Picco G, Gonçalves E, Beaver CM, Migliardi G, et al. Prioritization of
1158 cancer therapeutic targets using CRISPR–Cas9 screens. Nature. Nature Publishing Group;
1159 2019;568:511–6.

1160 15. Goodspeed A, Jean A, Costello JC. A Whole-genome CRISPR Screen Identifies a Role of
1161 MSH2 in Cisplatin-mediated Cell Death in Muscle-invasive Bladder Cancer. Eur Urol.
1162 2019;75:242–50.

1163 16. Huang A, Garraway LA, Ashworth A, Weber B. Synthetic lethality as an engine for cancer
1164 drug target discovery. Nat Rev Drug Discov. Nature Publishing Group; 2020;19:23–38.

1165 17. Jost M, Weissman JS. CRISPR Approaches to Small Molecule Target Identification. ACS Chem
1166 Biol. 2018;13:366–75.

1167 18. Olivieri M, Cho T, Álvarez-Quilón A, Li K, Schellenberg MJ, Zimmermann M, et al. A Genetic
1168 Map of the Response to DNA Damage in Human Cells. Cell. 2020;182:481-496.e21.

1169 19. Dobin A, Davis CA, Schlesinger F, Drenkow J, Zaleski C, Jha S, et al. STAR: ultrafast universal
1170 RNA-seq aligner. Bioinforma Oxf Engl. 2013;29:15–21.

1171 20. Robinson MD, McCarthy DJ, Smyth GK. edgeR: a Bioconductor package for differential
1172 expression analysis of digital gene expression data. Bioinforma Oxf Engl. 2010;26:139–40.

1173 21. Ritchie ME, Phipson B, Wu D, Hu Y, Law CW, Shi W, et al. limma powers differential
1174 expression analyses for RNA-sequencing and microarray studies. Nucleic Acids Res.
1175 2015;43:e47.

1176 22. Sergushichev AA. An algorithm for fast preranked gene set enrichment analysis using
1177 cumulative statistic calculation. bioRxiv. Cold Spring Harbor Laboratory; 2016;060012.

1178 23. Liberzon A, Subramanian A, Pinchback R, Thorvaldsdóttir H, Tamayo P, Mesirov JP.
1179 Molecular signatures database (MSigDB) 3.0. Bioinformatics. Oxford Academic;
1180 2011;27:1739–40.

1181 24. Wickham H. Ggplot2: elegant graphics for data analysis. New York: Springer; 2009.

1182 25. Gu Z, Eils R, Schlesner M. Complex heatmaps reveal patterns and correlations in
1183 multidimensional genomic data. Bioinformatics. 2016;32:2847–9.

1184 26. Robinson AE, Binek A, Venkatraman V, Searle BC, Holewinski RJ, Rosenberger G, et al. Lysine
1185 and Arginine Protein Post-translational Modifications by Enhanced DIA Libraries:
1186 Quantification in Murine Liver Disease. J Proteome Res. 2020;19:4163–78.

1187 27. Berle M, Ghila L, Vethe H, Chaudhry A, Garberg H, Beisland C, et al. Novel protein signatures
1188 suggest progression to muscular invasiveness in bladder cancer. PloS One.
1189 2018;13:e0206475.

1190 28. Parker SJ, Venkatraman V, Van Eyk JE. Effect of peptide assay library size and composition in
1191 targeted data-independent acquisition-MS analyses. Proteomics. 2016;16:2221–37.

1192 29. Parker SJ, Rost H, Rosenberger G, Collins BC, Malmström L, Amodei D, et al. Identification of
1193 a Set of Conserved Eukaryotic Internal Retention Time Standards for Data-independent
1194 Acquisition Mass Spectrometry. Mol Cell Proteomics MCP. 2015;14:2800–13.

1195 30. Röst HL, Rosenberger G, Navarro P, Gillet L, Miladinović SM, Schubert OT, et al.
1196 OpenSWATH enables automated, targeted analysis of data-independent acquisition MS
1197 data. Nat Biotechnol. 2014;32:219–23.

1198 31. Teleman J, Röst HL, Rosenberger G, Schmitt U, Malmström L, Malmström J, et al. DIANA--
1199 algorithmic improvements for analysis of data-independent acquisition MS data.
1200 Bioinforma Oxf Engl. 2015;31:555–62.

1201 32. Röst HL, Liu Y, D'Agostino G, Zanella M, Navarro P, Rosenberger G, et al. TRIC: an
1202 automated alignment strategy for reproducible protein quantification in targeted
1203 proteomics. Nat Methods. 2016;13:777–83.

1204 33. Choi M, Chang C-Y, Clough T, Broudy D, Killeen T, MacLean B, et al. MSstats: an R package
1205 for statistical analysis of quantitative mass spectrometry-based proteomic experiments.
1206 Bioinforma Oxf Engl. 2014;30:2524–6.

1207 34. Li H. Aligning sequence reads, clone sequences and assembly contigs with BWA-MEM.
1208 ArXiv13033997 Q-Bio [Internet]. 2013 [cited 2020 Oct 27]; Available from:
1209 http://arxiv.org/abs/1303.3997

1210 35. Faust GG, Hall IM. SAMBLASTER: fast duplicate marking and structural variant read
1211 extraction. Bioinforma Oxf Engl. 2014;30:2503–5.

1212 36. Sherry ST, Ward MH, Kholodov M, Baker J, Phan L, Smigielski EM, et al. dbSNP: the NCBI
1213 database of genetic variation. Nucleic Acids Res. 2001;29:308–11.

1214 37. 1000 Genomes Project Consortium, Auton A, Brooks LD, Durbin RM, Garrison EP, Kang HM,
1215 et al. A global reference for human genetic variation. Nature. 2015;526:68–74.

1216 38. Mills RE, Pittard WS, Mullaney JM, Farooq U, Creasy TH, Mahurkar AA, et al. Natural genetic
1217 variation caused by small insertions and deletions in the human genome. Genome Res.
1218 2011;21:830–9.

1219 39. Li H, Handsaker B, Wysoker A, Fennell T, Ruan J, Homer N, et al. The Sequence
1220 Alignment/Map format and SAMtools. Bioinformatics. 2009;25:2078–9.

1221 40. Okonechnikov K, Conesa A, García-Alcalde F. Qualimap 2: advanced multi-sample quality
1222 control for high-throughput sequencing data. Bioinforma Oxf Engl. 2016;32:292–4.

1223 41. Picard toolkit [Internet]. Broad Inst. GitHub Repos. Broad Institute; 2018. Available from:
1224 http://broadinstitute.github.io/picard/

1225 42. Benjamin D, Sato T, Cibulskis K, Getz G, Stewart C, Lichtenstein L. Calling Somatic SNVs and
1226 Indels with Mutect2. bioRxiv. Cold Spring Harbor Laboratory; 2019;861054.

1227 43. Wang K, Li M, Hakonarson H. ANNOVAR: functional annotation of genetic variants from
1228 high-throughput sequencing data. Nucleic Acids Res. 2010;38:e164–e164.

1229 44. Doench JG, Fusi N, Sullender M, Hegde M, Vaimberg EW, Donovan KF, et al. Optimized
1230 sgRNA design to maximize activity and minimize off-target effects of CRISPR-Cas9. Nat
1231 Biotechnol. 2016;34:184–91.

1232 45. Imkeller K, Ambrosi G, Boutros M, Huber W. gscreend: modelling asymmetric count ratios in
1233 CRISPR screens to decrease experiment size and improve phenotype detection. Genome
1234 Biol. 2020;21:53.

1235 46. Joung J, Konermann S, Gootenberg JS, Abudayyeh OO, Platt RJ, Brigham MD, et al. Genome-
1236 scale CRISPR-Cas9 knockout and transcriptional activation screening. Nat Protoc.
1237 2017;12:828–63.

1238 47. Winter J, Breinig M, Heigwer F, Brügemann D, Leible S, Pelz O, et al. caRpools: an R package
1239 for exploratory data analysis and documentation of pooled CRISPR/Cas9 screens.
1240 Bioinforma Oxf Engl. 2016;32:632–4.

1241 48. Love MI, Huber W, Anders S. Moderated estimation of fold change and dispersion for RNA-
1242 seq data with DESeq2. Genome Biol. 2014;15:550.

1243 49. Bates D, Mächler M, Bolker B, Walker S. Fitting Linear Mixed-Effects Models Using lme4. J
1244 Stat Softw. 2015;67:1–48.

1245 50. Kuznetsova A, Brockhoff PB, Christensen RHB. lmerTest Package: Tests in Linear Mixed
1246 Effects Models. J Stat Softw. 2017;82:1–26.

1247 51. Mullenders J, de Jongh E, Brousali A, Roosen M, Blom JPA, Begthel H, et al. Mouse and
1248 human urothelial cancer organoids: A tool for bladder cancer research. Proc Natl Acad Sci
1249 U S A. 2019;116:4567–74.

1250 52. Allory Y, Beukers W, Sagrera A, Flández M, Marqués M, Márquez M, et al. Telomerase
1251 reverse transcriptase promoter mutations in bladder cancer: high frequency across stages,
1252 detection in urine, and lack of association with outcome. Eur Urol. 2014;65:360–6.

1253 53. Hurst CD, Zuiverloon TCM, Hafner C, Zwarthoff EC, Knowles MA. A SNaPshot assay for the
1254 rapid and simple detection of four common hotspot codon mutations in the PIK3CA gene.
1255 BMC Res Notes. 2009;2:66.

1256 54. Junker K, van Oers JMM, Zwarthoff EC, Kania I, Schubert J, Hartmann A. Fibroblast growth
1257 factor receptor 3 mutations in bladder tumors correlate with low frequency of
1258 chromosome alterations. Neoplasia N Y N. 2008;10:1–7.

1259 55. Perez-Riverol Y, Csordas A, Bai J, Bernal-Llinares M, Hewapathirana S, Kundu DJ, et al. The
1260 PRIDE database and related tools and resources in 2019: improving support for
1261 quantification data. Nucleic Acids Res. 2019;47:D442–50.

1262 56. Vallo S, Michaelis M, Rothweiler F, Bartsch G, Gust KM, Limbart DM, et al. Drug-Resistant
1263 Urothelial Cancer Cell Lines Display Diverse Sensitivity Profiles to Potential Second-Line
1264 Therapeutics. Transl Oncol. 2015;8:210–6.

1265 57. Vallo S, Köpp R, Michaelis M, Rothweiler F, Bartsch G, Brandt MP, et al. Resistance to
1266 nanoparticle albumin-bound paclitaxel is mediated by ABCB1 in urothelial cancer cells.
1267 Oncol Lett. Spandidos Publications; 2017;13:4085–92.

1268 58. Robertson AG, Kim J, Al-Ahmadie H, Bellmunt J, Guo G, Cherniack AD, et al. Comprehensive
1269 Molecular Characterization of Muscle-Invasive Bladder Cancer. Cell. Elsevier;
1270 2017;171:540-556.e25.

1271 59. Landrum MJ, Lee JM, Benson M, Brown GR, Chao C, Chitipiralla S, et al. ClinVar: improving
1272 access to variant interpretations and supporting evidence. Nucleic Acids Res.
1273 2018;46:D1062–7.

1274 60. Korotkevich G, Sukhov V, Sergushichev A. Fast gene set enrichment analysis. bioRxiv. Cold
1275 Spring Harbor Laboratory; 2019;060012.

1276 61. Drayton RM, Catto JW. Molecular mechanisms of cisplatin resistance in bladder cancer.
1277 Expert Rev Anticancer Ther. Taylor & Francis; 2012;12:271–81.

1278 62. Galluzzi L, Senovilla L, Vitale I, Michels J, Martins I, Kepp O, et al. Molecular mechanisms of
1279 cisplatin resistance. Oncogene. 2012;31:1869–83.

1280 63. Huang D, Savage SR, Calinawan AP, Lin C, Zhang B, Wang P, et al. A highly annotated
1281 database of genes associated with platinum resistance in cancer. Oncogene.
1282 2021;40:6395–405.

1283 64. Dempster JM, Krill-Burger J, Warren A, McFarland JM, Golub TR, Tsherniak A. Gene
1284 expression has more power for predicting in vitro cancer cell vulnerabilities than
1285 genomics. bioRxiv. Cold Spring Harbor Laboratory; 2020;2020.02.21.959627.

1286 65. Chang Q, Ornatsky OI, Koch CJ, Chaudary N, Marie-Egyptienne DT, Hill RP, et al. Single-cell
1287 measurement of the uptake, intratumoral distribution and cell cycle effects of cisplatin
1288 using mass cytometry. Int J Cancer. 2015;136:1202–9.

1289 66. Tiriac H, Belleau P, Engle DD, Plenker D, Deschênes A, Somerville TDD, et al. Organoid
1290 Profiling Identifies Common Responders to Chemotherapy in Pancreatic Cancer. Cancer
1291 Discov. 2018;8:1112–29.

1292 67. Ooft SN, Weeber F, Dijkstra KK, McLean CM, Kaing S, van Werkhoven E, et al. Patient-
1293 derived organoids can predict response to chemotherapy in metastatic colorectal cancer
1294 patients. Sci Transl Med. 2019;11:eaay2574.

1295 68. Yao Y, Xu X, Yang L, Zhu J, Wan J, Shen L, et al. Patient-Derived Organoids Predict
1296 Chemoradiation Responses of Locally Advanced Rectal Cancer. Cell Stem Cell. 2020;26:17-
1297 26.e6.

1298 69. de Witte CJ, Espejo Valle-Inclan J, Hami N, Lõhmussaar K, Kopper O, Vreuls CPH, et al.
1299 Patient-Derived Ovarian Cancer Organoids Mimic Clinical Response and Exhibit
1300 Heterogeneous Inter- and Intrapatient Drug Responses. Cell Rep. 2020;31:107762.

1301 70. Reid AHM, Protheroe A, Attard G, Hayward N, Vidal L, Spicer J, et al. A First-in-Man Phase I
1302 and Pharmacokinetic Study on CHR-2797 (Tosedostat), an Inhibitor of M1
1303 Aminopeptidases, in Patients with Advanced Solid Tumors. Clin Cancer Res. 2009;15:4978–
1304 85.

1305 71. Chargi N, Molenaar-Kuijsten L, Huiskamp LFJ, Devriese LA, de Bree R, Huitema ADR. The
1306 association of cisplatin pharmacokinetics and skeletal muscle mass in patients with head
1307 and neck cancer: The prospective PLATISMA study. Eur J Cancer Oxf Engl 1990.
1308 2022;160:92–9.

1309 72. Urien S, Lokiec F. Population pharmacokinetics of total and unbound plasma cisplatin in
1310 adult patients. Br J Clin Pharmacol. 2004;57:756–63.

1311 73. Cortes J, Feldman E, Yee K, Rizzieri D, Advani AS, Charman A, et al. Two dosing regimens of
1312 tosedostat in elderly patients with relapsed or refractory acute myeloid leukaemia (OPAL):
1313 a randomised open-label phase 2 study. Lancet Oncol. 2013;14:354–62.

1314 74. Löwenberg B, Morgan G, Ossenkoppele GJ, Burnett AK, Zachée P, Dührsen U, et al. Phase
1315 I/II clinical study of Tosedostat, an inhibitor of aminopeptidases, in patients with acute
1316 myeloid leukemia and myelodysplasia. J Clin Oncol Off J Am Soc Clin Oncol. 2010;28:4333–
1317 8.

1318 75. Hanada K, Nishijima K, Ogata H, Atagi S, Kawahara M. Population pharmacokinetic analysis
1319 of cisplatin and its metabolites in cancer patients: possible misinterpretation of covariates
1320 for pharmacokinetic parameters calculated from the concentrations of unchanged
1321 cisplatin, ultrafiltered platinum and total platinum. Jpn J Clin Oncol. 2001;31:179–84.

1322 76. Constam DB, Tobler AR, Rensing-Ehl A, Kemler I, Hersh LB, Fontana A. Puromycin-sensitive
1323 aminopeptidase. Sequence analysis, expression, and functional characterization. J Biol
1324 Chem. 1995;270:26931–9.

1325 77. Menzies FM, Hourez R, Imarisio S, Raspe M, Sadiq O, Chandraratna D, et al. Puromycin-
1326 sensitive aminopeptidase protects against aggregation-prone proteins via autophagy. Hum
1327 Mol Genet. 2010;19:4573–86.

1328 78. Saric T, Graef CI, Goldberg AL. Pathway for degradation of peptides generated by
1329 proteasomes: a key role for thimet oligopeptidase and other metallopeptidases. J Biol
1330 Chem. 2004;279:46723–32.

1331 79. Towne CF, York IA, Neijssen J, Karow ML, Murphy AJ, Valenzuela DM, et al. Puromycin-
1332 Sensitive Aminopeptidase Limits MHC Class I Presentation in Dendritic Cells but Does Not
1333 Affect CD8 T Cell Responses during Viral Infections. J Immunol. 2008;180:1704–12.

1334 80. Karsten SL, Sang T-K, Gehman LT, Chatterjee S, Liu J, Lawless GM, et al. A genomic screen
1335 for modifiers of tauopathy identifies puromycin-sensitive aminopeptidase as an inhibitor
1336 of tau-induced neurodegeneration. Neuron. 2006;51:549–60.

1337 81. Kudo LC, Parfenova L, Ren G, Vi N, Hui M, Ma Z, et al. Puromycin-sensitive aminopeptidase
1338 (PSA/NPEPPS) impedes development of neuropathology in hPSA/TAU(P301L) double-
1339 transgenic mice. Hum Mol Genet. 2011;20:1820–33.

1340 82. Schönlein C, Löffler J, Huber G. Purification and characterization of a novel metalloprotease
1341 from human brain with the ability to cleave substrates derived from the N-terminus of
1342 beta-amyloid protein. Biochem Biophys Res Commun. 1994;201:45–53.

1343 83. Yanagi K, Tanaka T, Kato K, Sadik G, Morihara T, Kudo T, et al. Involvement of puromycin-
1344 sensitive aminopeptidase in proteolysis of tau protein in cultured cells, and attenuated
1345 proteolysis of frontotemporal dementia and parkinsonism linked to chromosome 17
1346 (FTDP-17) mutant tau. Psychogeriatrics. 2009;9:157–66.

1347 84. Karczewski KJ, Francioli LC, Tiao G, Cummings BB, Alföldi J, Wang Q, et al. The mutational
1348 constraint spectrum quantified from variation in 141,456 humans. Nature. 2020;581:434–
1349 43.

1350 85. Uhlen M, Zhang C, Lee S, Sjöstedt E, Fagerberg L, Bidkhori G, et al. A pathology atlas of the
1351 human cancer transcriptome. Science. 2017;357.

1352 86. Osada T, Ikegami S, Takiguchi-Hayashi K, Yamazaki Y, Katoh-Fukui Y, Higashinakagawa T, et
1353 al. Increased anxiety and impaired pain response in puromycin-sensitive aminopeptidase
1354 gene-deficient mice obtained by a mouse gene-trap method. J Neurosci Off J Soc Neurosci.
1355 1999;19:6068–78.

1356 87. Hitzerd SM, Verbrugge SE, Ossenkoppele G, Jansen G, Peters GJ. Positioning of
1357 aminopeptidase inhibitors in next generation cancer therapy. Amino Acids. 2014;46:793–
1358 808.

1359 88. Krige D, Needham LA, Bawden LJ, Flores N, Farmer H, Miles LEC, et al. CHR-2797: an
1360 antiproliferative aminopeptidase inhibitor that leads to amino acid deprivation in human
1361 leukemic cells. Cancer Res. 2008;68:6669–79.

1362 89. van Herpen CML, Eskens F a. LM, de Jonge M, Desar I, Hooftman L, Bone EA, et al. A Phase
1363 Ib dose-escalation study to evaluate safety and tolerability of the addition of the
1364 aminopeptidase inhibitor tosedostat (CHR-2797) to paclitaxel in patients with advanced
1365 solid tumours. Br J Cancer. 2010;103:1362–8.

1366 90. Mawad R, Becker PS, Hendrie P, Scott B, Wood BL, Dean C, et al. Phase II study of
1367 tosedostat with cytarabine or decitabine in newly diagnosed older patients with acute
1368 myeloid leukaemia or high-risk MDS. Br J Haematol. 2016;172:238–45.

1369 91. Sachs N, de Ligt J, Kopper O, Gogola E, Bounova G, Weeber F, et al. A Living Biobank of
1370 Breast Cancer Organoids Captures Disease Heterogeneity. Cell. 2018;172:373-386.e10.

1371 92. Lee SH, Hu W, Matulay JT, Silva MV, Owczarek TB, Kim K, et al. Tumor Evolution and Drug
1372 Response in Patient-Derived Organoid Models of Bladder Cancer. Cell. 2018;173:515-
1373 528.e17.

1374